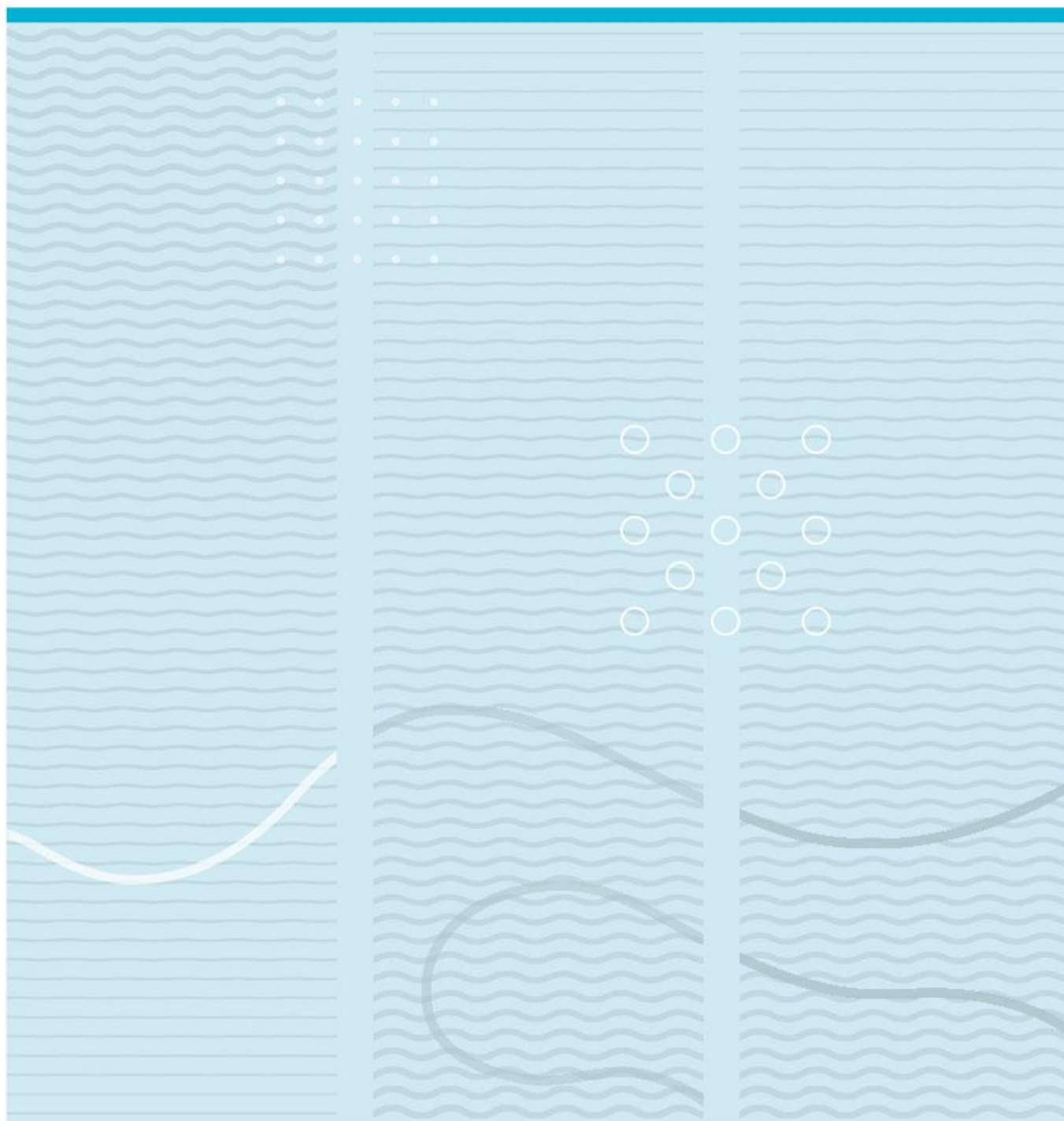


Sharaban Tahora

Fabrication of phantom skin for the biomedical test



University of South-Eastern Norway
Faculty of Technology, Natural Sciences and Maritime Sciences
Institute of Microsystems
Raveien 215
NO-3184 Borre, Norway

<http://www.usn.no>

© 2021 Sharaban Tahora

Abstract

Implantable biomedical devices (IMDs) have an enormous prospect in the medical sector. A phantom skin model with similar properties to human skin can be fabricated to analyze if the exchange of energy between the IMD and external devices can produce any effect on the skin of the patient. This analysis can provide numerous information before implanting the IMD in humans and animals.

This project aims to fabricate a phantom skin model with similar electrical and acoustic properties to human skin to test IMDs. The fabrication methodology is based on the agar/gelatin gel with other chemicals to replicate some properties of human skin, such as conductivity, speed of sound (SOS), and attenuation coefficient.

An agar-based gel with NaCl solution was prepared to replicate the electrical properties, which was validated with a conductivity meter probe. For the acoustic model of human skin, agar/gelatin powder was used to prepare the gel with other chemical substances. Among the others, bovine serum albumin (BSA), methanol, glutaraldehyde were expected to provide the best results. To compare the multilayer and homogeneous phantom models, both types of phantom skins were fabricated. Later the characterization of the acoustic properties was done with piezoelectric transducers in a water tank setup.

Due to the closure of the lab, all the experiments were not completed. Therefore, the electrical and acoustic properties in one single phantom model could not be achieved. Further experiments can be conducted to achieve this goal and to have improved received signals for calculating the speed of sound.

Contents

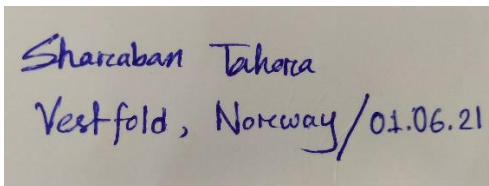
Abstract.....	3
Contents.....	5
Foreword.....	7
1 Introduction	8
1.1 Objectives.....	10
2 State of the art of phantom skin	12
3 Background theory	14
3.1 Human skin properties	14
3.1.1 Electrical properties.	16
3.1.2 Mechanical properties.....	16
3.1.3 Optical properties.....	16
3.1.4 Acoustic properties.	17
3.3 Conductivity calculation	17
3.4 Electrical modelling	18
4 Method	21
4.1 Phantom skin with electrical properties.....	21
4.1.1 NaCl solution preparation	21
4.1.2 Agar gel preparation.....	23
4.2 Conductivity measurement	24
4.3 Phantom skin with acoustic properties	25
4.3.1 Fabrication of layered phantom skin.....	26
4.3.2 Fabrication of homogeneous phantom skin.....	28
4.4 Setup for the characterization of acoustic properties of phantom skin.....	30
4.4.1 Selection of the transducer.	30
4.4.2 Insulation with Polydimethylsiloxane (PDMS)	31
4.4.3 The resonance frequency of the transducer	33
4.4.4 Driver for ultrasound transducer.....	34
4.4.5 Measurement of acoustic properties	35
5 Materials.....	38
5.1 Consumable.....	38
5.2 Tools and devices	38

6	Result and discussion	39
6.1	The conductivity of phantom skin	39
6.2	Resonance frequency	41
6.3	Speed of sound (SOS) of phantom skin	44
6.4	Attenuation coefficient of phantom skin	49
6.5	Proposed multilayer phantom skin model with acoustic and electrical properties.....	53
6.6	Challenges and suggestions.....	55
8	Conclusion	58
	References	60
	List of figures	64
	List of tables.....	66
	Appendix	67

Foreword

This is the final project of my master's study in micro and nano systems technology. Several people helped me in reaching this final point of my study. First of all, I would like to thank my supervisor Luca Marchetti who has been very supportive throughout my thesis. I would also like to thank Dr. Birgitte Kasin Hønsvall, who has been very helpful during my chemical experiments in the USN lab.

I would especially like to thank Even Zimmer, Dr. Martin Peacock, and Linhongjia Xiong for allowing me to perform some chemical experiments inside the cleanroom of Zimmer & Peacock Ltd. During the special situation of COVID, it helped me to continue my research work. I would also like to thank my friends and family for supporting me all the time.

A photograph of a handwritten note on a light-colored surface. The text is written in blue ink and reads: "Sharaban Tahora" on the first line, and "Vestfold, Norway / 01.06.21" on the second line.

Sharaban Tahora

1 Introduction

With the advancement of electronic devices, especially in miniaturized technology, medical science has accomplished numerous significant and easy ways for healthcare. Nowadays, Implantable biomedical devices (IMDs) are an essential part of medical diagnosis, prognosis, therapeutic, or research for different inspections that can be implanted partially or entirely inside human or animal bodies. IMDs can help reach unreachable locations inside the human body such as skin, heart, brain, spinal cord, eye, intravascular regions, cells, etc. [1].

IMDs can be independent without external power sources or dependent on power supplied from external sources [1]. The independent IMDs may have one-time batteries such as lithium, nuclear, etc., whereas examples of environmental harvesting sources are biofuel cells, thermoelectricity, piezoelectricity, electrostatics, and electromagnetics [1]. Independent IMDs provide an easy solution by avoiding any complex procedure. However, it's not entirely reliable in supplying continuous power to the system; it can make patients' lives miserable because it may require changing the battery or power supply regularly, which may involve risky operations in some cases [2]. Therefore, wireless transfer energy system between IMDs and external power sources has drawn attention to many researchers. This technique can provide an alternative way to supply power to the implanted device or recharge the battery.

Different techniques can be used to exchange energy between IMD and external devices, such as radio frequency (RF) [3], ultrasound transducers, inductive coupling, etc. [1]. Wireless energy transfer between IMDs and external devices helps to supply the required energy to run the system. Furthermore, the same wireless system can be used to implement a communication medium between the IMD and remote monitoring systems. The latter can be used to monitor any internal injury so that doctors can provide the proper medication by monitoring the healing process. Among the above-mentioned wireless communication systems, RF and ultrasound transducers are reliable compared to inductive coupling because both the coils of an inductive coupling need to be aligned to transfer energy efficiently. Moreover, a miniature version of thin coil fabrication is another challenge for researchers [1]. On the other hand, RF energy transfer uses an

antenna to employ the best wireless communication to harvest energy, and an antenna can also be employed on the circuit chip [4]. Ultrasonic transducers are also popular for transferring energy between IMD and external devices [5], [6].

Table 1: Comparison between ultrasound and RF energy transfer methods

Advantages & disadvantages of the ultrasound energy system [1], [7]	Advantages & disadvantages of the RF energy system [3]
<ul style="list-style-type: none"> • It is efficient, smaller in size, safe, and does not cause any harm due to other electromagnetic effects. • It can be powered with an external ultrasonic transducer either with capacitance mode or piezoelectric mode. • It can be designed compactly with micro nano electrical mechanical systems (MEMS) technology. • Capacitive and piezoelectric ultrasonic transducers require high and low voltages, respectively; therefore, the latter is suitable. • The operating frequency can be in the megahertz (MHz) range to transfer energy. • It is easy to choose the operating wavelength for ultrasonic systems, and the long-wavelength energy can penetrate the deeper area in the human body. • It can cause cavitation in the human body, which may lead to several side effects. 	<ul style="list-style-type: none"> • It is efficient and smaller in size. • It can be designed compactly with MEMS technology. • In the RF system, the ambient RF signals can be transformed into electrical signals with the antenna. • It can be used remotely for having an antenna. • The operating frequency to transfer energy is much higher than the ultrasonic energy system. • There are enormous RF sources present in the environment which can be used for energy harvesting. • It has lower power, high losses, and its radiation is harmful to the human body.

Table 1 has discussed the advantages and disadvantages of ultrasound and RF energy systems. Overall, the two technologies have pros and cons. Thus, it is possible that a hybrid solution may be the best technology to employ.

IMDs have great potential in the biomedical sector as they can minimize the suffering of patients in different treatment and monitoring processes. Any biomedical device needs to be adequately tested due to restrictions on testing any novel device directly on the human body. Therefore, for IMDs, the impact of the new device needs to be assured before implanting it in the human body [8]. An animal testing model is a traditional way for laboratory testing before launching the device. In some cases, it is also restricted to test the device on animals as it requires specific criteria to be fulfilled [9], [10]. Although animal tests are an excellent human biology model, the test results on animals are not always reliable for humans [11].

Moreover, testing a device on humans and animals can be very costly and time-consuming as it requires several procedures to be fulfilled. Phantom tissues are good models of human skin that can be fabricated for implantable biomedical device testing. Phantom skin is an artificial skin fabricated in a laboratory to simulate actual human tissues' mechanical, electrical, optical, or acoustic properties. The study of skin properties is essential to fabricate phantom tissue to understand the energy transfer between IMD and external devices. Moreover, it helps to understand the effect of energy flowing through human skin as it may cause some damages to the skin.

Nowadays, phantom skins are available commercially [12], [13]. However, no available phantom skins serve all aspects of human skin properties. Therefore, a lot of researches are going on in this field [14]–[18]. Especially the multilayer skin model is a novel field of study which consists of stacking multiple layers, each one with different skin characteristics. In this way, the complex properties of the human skin can be achieved. RF and ultrasound wireless energy transfer systems are considered for this project; therefore, human skin conductivity and acoustic properties are the prime study focus here.

1.1 Objectives

The purpose of this thesis work is to fabricate multilayer phantom skin having similar electrical and acoustic properties to human skin. This accomplishment will help to realize a measurement setup for the characterization of wireless transfer energy techniques

between an IMD and an external energy source. At first, the phantom skins with electrical and acoustic properties were fabricated separately. Afterward, both the models are supposed to be combined in one recipe to see if it's possible to have both characteristics in one phantom model. The characterization of the electrical properties was completed with a conductivity meter. On the other hand, the acoustic properties characterization included calculating the attenuation coefficient and the speed of sound of different phantom skins among all acoustic properties due to time constraints. The characterization of acoustic properties was conducted with two piezoelectric transducers.

2 State of the Art of Phantom Skin

Tissue mimicking research is fundamental in biomedical engineering. Since 1960, it has been used in ultrasound imaging [19]. A medical ultrasonic transducer comprises either single-element or multiple elements that can capture high-frequency sound [16]. In biomedical engineering, phantom samples are used with known properties and geometry, which helps to characterize a new device model.

Human skin has several properties such as electrical, mechanical, optical, acoustic, etc. For ultrasound signal communication research, a measurement study of acoustic properties of human skin is necessary. The acoustic properties of human skin rely on acoustic attenuation, backscattering, mass density, speed of sound, acoustic impedance, etc. For RF communication research, electrical properties need to be studied, which relies on conductivity. Therefore, phantom tissues with human skin properties can be fabricated by replicating the different properties of human skin.

There are different approaches to fabricate phantom skin with acoustic properties. Many materials and techniques have been used to replicate the acoustic properties of human tissue. Some tried to develop a homogeneous material, and some attempted to fabricate a layer-by-layer model [15], [20], [21]. On the other hand, to replicate human skin conductance, a standard method is to use salt solution with agar gel [22].

Homogeneous phantom tissue is a bulk and intrinsic material that consists of the properties of human tissue. In the multilayer tissue-mimicking process, usually, layer-by-layer tissue phantoms are fabricated using a mold. Each layer may vary in the concentration of different chemicals.

The most common material for a tissue-mimicking phantom is agar and gelatin. These two gels are easy to prepare and non-hazardous. Moreover, they are prepared with deionized water (DI), which contains similar acoustic properties to human skin. Agar/gelatin gel is sometimes breakable, and the strength may lessen with the increase in temperature. Moreover, it is important to store these gel phantoms in a sterile environment, which is related to long-term usage and stability. A long-term stable

material is essential while measuring the properties and test applications. Different cross-linker or hardener can be used to avoid this problem, such as glutaraldehyde, formaldehyde, etc. [15], [16], [23], [24]. Alternative ways to use a hardener are increasing the amount of powder in gel preparation or heating the gel solution at a higher temperature for a longer time, for example, boiling the solution for 20 minutes at 95°C [17]. Both agar and gelatin are not good acoustic attenuators [15]. Therefore, different acoustic attenuators can be used to modify the attenuation coefficient of the phantom skin, such as bovine serum albumin (BSA), graphite, aluminium oxide (Al_2O_3), etc. [15], [19], [23]–[25]. BSA is a protein that has been widely used to modify acoustic attenuation, and it helps increase the attenuation linearly with its increasing percentage in the solution. BSA should be added to agar/gelatin solution lower than its denaturing temperature [25], [26]. It was also reported that increasing the concentration of graphite in the solution can increase the attenuation coefficient [27]. Acoustic attenuation is also dependent on frequency. Therefore, using a transducer with a 1-2 MHz range will give the correct attenuation value of approximately 0.5 to 3.3dB/cm/MHz for soft tissues [17]. The common modifiers for backscattering coefficient are silica beads, polystyrene, copolymer microspheres, etc. [15], [16], [23], [25]. The backscattering coefficient tends to increase with the increasing concentration of glass beads in the solution. The speed of sound (SOS) of agar/gelatin-based phantom skin depends on various aspects. Already agar and gelatin solutions prepared with water have the SOS and impedance close to the water, which is close to the human skin. In addition to each percentage of gelatin and agar, the SOS increases by 3.2ms^{-1} and 10ms^{-1} , respectively [15]. Other chemicals also help to modify the SOS of the phantom skin, such as BSA, N-propanol, ethanol, methanol, etc. [15], [23], [24], [27]. To avoid microbial contamination, german plus, p-methyl, p-propyl benzoin, benzalkonium chloride, etc., can be used [15], [19], [28].

Other chemicals to fabricate tissue-mimicking phantom are polyacrylamide (PAA), polyvinyl alcohol (PVA), silicone, etc. In PVA gel phantom, glycol and alumina powder can be added to achieve expected SOS, attenuation, and backscattering [20]. PVA gel has a similar texture to human tissue, and it has long-term stability compared to agar/gelatin-based phantom. It is easy to prepare and low cost, but it is a time-consuming process as it requires a freezing cycle of 24 hours to cross-link [19], [20], [29]. PAA gel can be

prepared using acrylamide monomer; however, it is a harmful material and needs precautions [19]. Silicone-based phantom has more stability and longevity; however, it is challenging to achieve desired SOS and attenuation [19].

To replicate the conductivity of human skin, NaCl is the most used chemical, and it is easy to prepare with agar gel [22].

3 Background theory

Before fabricating the phantom skin, it is essential to study the properties of human skin. Afterward, focused human skin properties can be replicated and characterized with different chemicals and instruments.

3.1 Human skin properties

For biomedical research and treatment, human skin and tissue study is necessary. Human tissue can be categorized into two forms, soft and hard. Examples of human soft tissues are skin, vessels, blood, breast tissue, brain tissue, bladder tissue, cardiac tissue, liver tissue, etc. Human skin has three layers shown in figure 1; the outermost layer of the skin, which provides a waterproof barrier, is known as the epidermis, and it also generates the skin tone, dermis located under the epidermis layer, which contains connective tissue, hair follicles, sweat glands, etc., and hypodermis is made of fat and connective tissue [30].

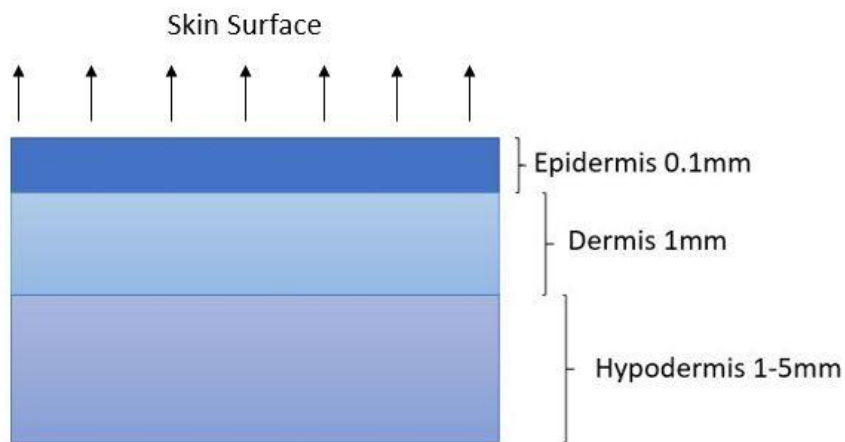


Figure 1: Human skin layers with thickness

The thickness of the epidermis, dermis, and hypodermis are 0.1mm, 1mm, and 1-5mm, respectively [15]. Thickness depends on the human body's location, and it also varies with human age, gender, skin type, etc. Table 2 displays the variation of the human skin layer's thickness which refers to the human forearm [15], [31].

Table 2: Thickness of different skin layers [15], [31]

Tissue layer	Body location	Thickness (mm)
Epidermis	Forearm	0.75 – 0.138
Dermis	Forearm	0.92 – 1.350
Hypodermis	Forearm	1.21 – 2.15

3.1.1 Electrical properties

Conductivity is the measure of electrical property in human skin. The conductivity of human tissue can vary with different criteria such as tissue type, location, etc. Human dry skin, wet skin, fat tissue, muscle have conductivity 0.68956, 0.6702, 0.04117, and 0.79721 siemens per meter (S/m), respectively [32]. However, the conductivity also changes with sweat. Other papers investigating human skin conductivity showed some deviations in these values [18], [22]. Some also mentioned the conductivity of each layer of human skin [33]. Although electrical conductivity and dielectric constant are independent of each other, it is also necessary to evaluate the dielectric properties of human tissue to characterize the electrical properties of human skin [34], [35]. There are two established mathematical models for the dielectric response of biological tissues, multi-debey dispersion and multi-cole dispersion [35]. However, due to the time limit, the characterization of the dielectric constant of phantom skin could not be investigated in this thesis.

3.1.2 Mechanical properties

Mechanical properties of human skin mainly depend on Young's modulus and shear modulus. Young's and shear modulus present the elasticity and the rigidity of a material. In human tissue, mechanical properties are influenced by keratin, collagen/elastin, and adipose in the epidermis, dermis, and hypodermis, respectively [15].

3.1.3 Optical properties

The optical properties of human skin mainly depend on absorption and scattering. These properties depend on Melanin, collagen/elastin, adipose/hemoglobin in the epidermis, dermis, and hypodermis, respectively [15].

3.1.4 Acoustic properties

Attenuation coefficient, backscatter coefficient, speed of sound, acoustic impedance, and mass density are the main factors to evaluate the acoustic properties [4], [6], [8], [9]. Skin layers have various constituents to have different acoustic properties. Keratin/melanin, collagen/elastin, and adipose are responsible for all the acoustic properties of the epidermis, dermis, and hypodermis, respectively [15].

The loss of energy while passing through a material is known as attenuation. Therefore, it is possible to measure how an ultrasound signal can easily pass through a material with an attenuation coefficient. Backscattering is the part of a wave or signal that reflects in all directions after striking an object. Mass density is a measure of the mass and volume of the material. An acoustic impedance is a measure of signal or beam resistance when it passes an object.

3.2 Electrical conductivity calculation

The study or replication of electrical properties of human skin is necessary if the communication media between implanted and external device is RF signal. RF signal is generated when an alternating current or voltage passes through conductive media [36], [37]. Thus, phantom skin with similar conductivity to human skin is highly desirable to send an RF signal through the sample. Electrical conductivity is the studied parameter in determining electrical properties for this research, and the conductivity was measured for liquid or semi-liquid materials. Few factors control the conductivity in a solution, such as concentration, mobility of ions, the valence of ions, temperature, etc. [38]. The ionic components that help to make the solution conductive are known as electrolytes [39]. Conductivity can be measured either using a conductivity meter which allows to measure it directly in Siemens per meter (S/m), or measure the resistivity in Ohms (Ω) and later convert it into conductance in Siemens (S) following the equation (1). Then, conductivity can be calculated by dividing the distance between electrodes/probes.

$$\sigma = \frac{1}{\rho} \quad (1)$$

A phantom skin with similar conductivity to human skin can be fabricated using agar gel, DI water, and NaCl solution. NaCl can control the conductivity of different skin layers. DI water is very low conductive or sometimes non-conductive, whereas agar solution can be little conductive compared to DI water. This observation was found by D. Bannet, and based on this observation, a relationship formula between salt concentration and the conductivity of agar gel was proposed, which is given in the following equation (2) [22]. In this formula, 0.0529S/m is the additional conductivity that comes from the agar solution[22].

$$\sigma (S/m) = 215 \times \frac{(\text{grams of NaCl})}{(\text{soluiton volume in ml})} + 0.0529 \quad (2)$$

3.3 Electrical modelling

For the characterization of acoustic properties, piezoelectric disc transducers can be used. These are electromechanical devices, which require a Multiphysics simulator such as COMSOL to simulate their behavior. Nevertheless, electronic engineers found out a simple method to mimic the behavior of a piezoelectric transducer by using simple electrical lumped elements. The electrical model of transmitter and receiver transducers is given in figure 2. Moreover, the same electrical model can be used for RF antennas. Therefore, the circuit model given in figure 2 is valid for both ultrasound transducer and RF antenna.

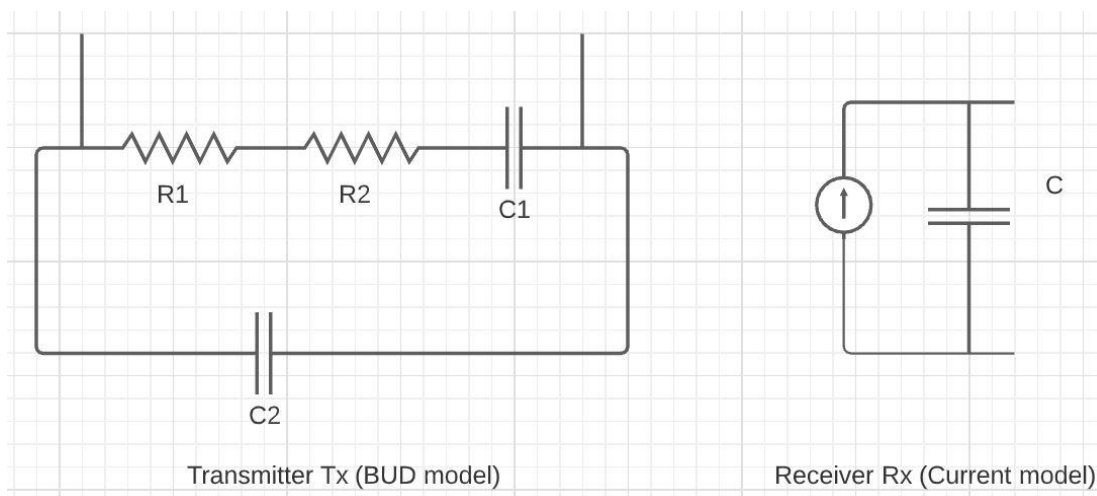


Figure 2: Electrical model of the ultrasound transducer and RF antenna

The main advantage of this equivalent electrical model is that it can be analyzed with a simple SPICE simulator. The mode of energy vibration is another vital feature to consider to transmit a signal with a transducer. A disc transducer can vibrate both axially and radially shown in figure 3. For this experiment, axial vibration is the method of consideration to send the signal.

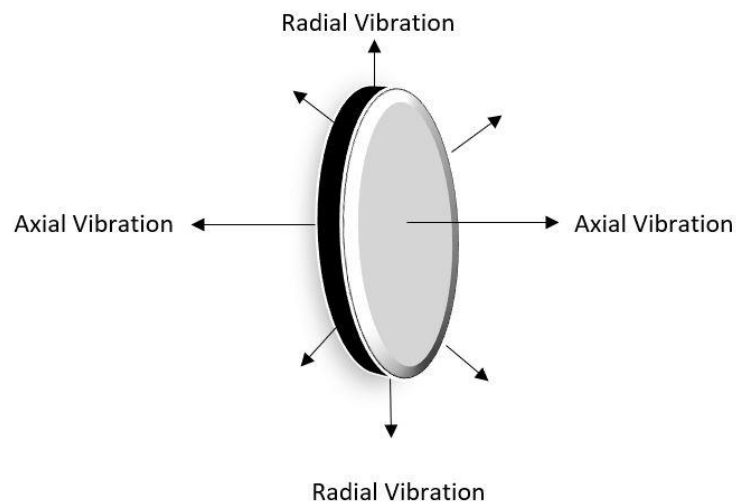


Figure 3: Vibration mode of piezoelectric disc transducer

The function of a transducer is mainly to convert energy from one form to another. A piezoelectric transducer can be represented with an equivalent RLC circuit model, which consists of a resistor (R), an inductor (L), and a capacitor (C). This circuit model is called a resonant circuit, which has low impedance at resonance frequency [40]. In an ideal piezoelectric transducer, the impedance of the transducer becomes resistive at the resonance frequency, and it is assumed to be the minimum value. To avoid power loss in the transducer, an inverting driver is helpful. The driver allows to maximize the power transfer toward the transmitter; therefore, it will enable receiving more power at the receiver side. The circuit diagram of the driver with the transducer is given in figure 4. The driver consists of three inverters inside, and two are used to drive the transducer by generating two opposite signals. In this way, the voltage across the transducer will oscillate with a peak to peak voltage equal to $2V_D$.

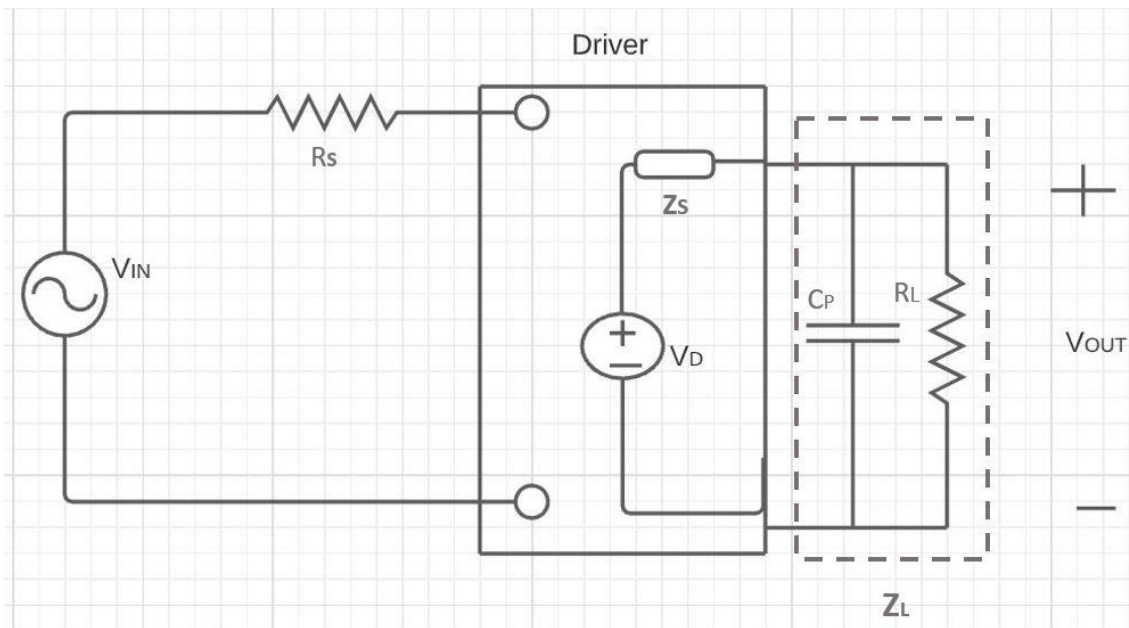


Figure 4: Circuit diagram of transmitting transducer connected to the driver

For maximum power transfer, the impedance of the transmitting transducer is the complex conjugate impedance of the driver ($Z_L = Z_s^*$).

4 Method

The method part of this thesis includes several experimental sections. First of all, the phantom samples were prepared, and later the samples were characterized with the arranged set up in the lab with different instruments for electrical and acoustic measurement.

4.1 Phantom skin with electrical properties

To establish a similar conductivity as human skin, a lab experiment has been conducted by following the paper 'Skin Conductivity Hydration Monitoring for Wearable Devices' by Mads Fredrik Walaas. NaCl solution has been used to control phantom skin conductivity, which can also replicate the human sweat conductivity.

4.1.1 NaCl solution preparation

For preparing NaCl solution, concentration calculation of different molarity should be done. The molarity calculation of the stock solution (the solution with the highest concentration) and solution dilution can be determined by equations (3) and (4), respectively.

$$\text{Molarity (mol/L)} = \frac{\text{moles of solute}}{\text{liters of solution}} \quad (3)$$

$$C_1V_1 = C_2V_2 \quad (4)$$

In equation (4), C_1 , C_2 , V_1 and V_2 are the stock solution concentration, final concentration, stock solution volume, and final solution volume.

This process was performed inside the biology lab. At first, 3.99g NaCl powder was dissolved into 200ml of DI water to prepare the stock NaCl solution of 342 millimolar (mMol). In this case, the selected stock solution molarity and solution amount are 342mMol and 200ml, respectively. Therefore, the moles of solute can be calculated from equation (3), which is 0.0684mol. Since the molecular weight for NaCl is 58.44g/mol (this is given in the chemical chart of the provider company), the required weight for

0.0684mol of NaCl is 3.99g. Later the solution was placed onto a magnetic hot plate to have continuous stirring to get a clear mixture. Afterward, 171mMol, 85mMol, and 42mMol NaCl solutions were prepared, shown in figure 5, and the preparation composition is given in table 3. This dilution calculation can be verified by equation (4). The solutions were prepared by diluting the prior stock solution to change the molarity. For example, the stock solution concentration is 342mMol, and 171mMol solution can be prepared by diluting the stock solution. To prepare 40ml of diluted solution of 171mMol NaCl, 20ml of stock solution, and 20ml of DI water will be mixed together. In the same dilution process, other solutions were also prepared. However, in the range of small concentrations, a slight deviation may occur [41]. This lab work was concentrated only on replicating a reproducible phantom skin with similar conductivity to human skin, which does not require a very low molarity of the salt solution. Therefore, the deviations in small concentration solutions were not verified here.

Table 3: Chemical composition of phantom skin to obtain target conductivity

Solution	Amount of NaCl (g)	Amount of DI water (ml)	Dilution method from the stock solution (ml)	Concentration of NaCl solution (mMol)	Expected conductivity (mS/cm) [41]
1	3.99	200	0	342	30.2
2	-	20	20	171	16
3	-	20	20	85	8.2
4	-	20	20	42	4.1



Figure 5: NaCl solution with different concentrations, and the calculation is given in table 2

4.1.2 Agar gel preparation

The whole process was performed inside the biology lab. Agar gel solutions were prepared in four different beakers, and each beaker contained 13.5ml of DI water and 0.405g of agar powder [22], [41]. Later these solutions were mixed with NaCl solutions with different concentrations given in table 4, and the amount of the NaCl solution was 13ml for all. At first, agar powder was weighed approximately 0.405g, and 13.5ml of DI water was added. Then, the beaker was rested on the magnetic hot plate at 200°C with a stirring speed of 250 to 300 rpm for about 6 minutes until the solution started to boil and dissolved completely. At that time, about 13ml of NaCl from each of the solutions was added to the specified agar solution beakers. The prepared solutions were kept at room temperature to form gels displayed in figure 6. It took approximately one hour to set the gels properly. The resistance was measured immediately with the multimeter shown in figure 7 and converted to conductivity afterward.

Table 4: Agar gel preparation with NaCl solution

Concentration of NaCl solution (mMol)	NaCl solution (ml)	Agar Solution (ml)	Expected conductivity (mS/cm) [41]
342	13	13.5	30.2
171	13	13.5	16
85	13	13.5	8.2
42	13	13.5	4.1

A similar preparation of agar gel was repeated with a variation in the amount of NaCl solution to see the differences in conductivity. This time the conductivity was measured with a conductivity meter probe.



Figure 6: Agar gel with NaCl

4.2 Conductivity measurement

In the beginning, the multimeter shown in figure 7 was used to measure the conductivity. This device measures the resistance, which is possible to convert into conductivity. The resistance of each agar solution was recorded at 65°C. The probe distance affects the conductivity calculation; thus, both the probes were bound together with parafilm to achieve a fixed space for all the measurements. The distance between probes was approximately 2cm which was measured with a ruler.

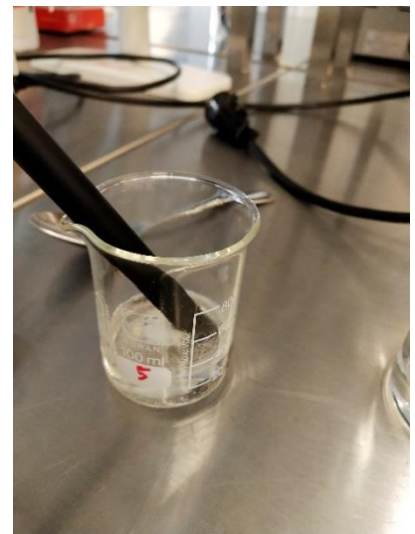


Figure 7: Multimeter used for resistance measurement

The same experiment was repeated as the multimeter reading was not as expected. Later, the conductivity was measured with a conductivity meter probe shown in figure 8, which provided the confirmation with the desired conductivity range.



(a)



(b)

Figure 8: (a) Conductivity meter, (b) Measuring the conductivity of the solution with the probe

4.3 Phantom skin with acoustic properties

There is a necessity of replicating the acoustic properties of human skin to transfer energy between implanted and external devices through ultrasound transducers. The acoustic

properties of human skin depend on the speed of sound (SOS), attenuation coefficient, backscatter coefficient, and acoustic impedance. This fabrication method mainly focuses on fabricating a multilayer phantom model with similar acoustic properties to human skin to see the difference in measured results with homogeneous phantom skin.

4.3.1 Fabrication of layered phantom skin

In this experiment, three different layers of phantom skin, such as epidermis, dermis, and hypodermis, have been fabricated with various chemicals to replicate the acoustic properties of human skin. Here, the focused acoustic properties are the attenuation coefficient and the speed of sound.

The whole process was performed inside Zimmer & Peacock cleanroom with proper precautions and safety measures. In this method, the layers of phantom skin were prepared with different chemicals as separate layers. The whole experiment was conducted inside the fume hood.

The attenuation coefficient and speed of sound of the epidermis layer are dominated by keratin/melanin in human skin, which can be replicated using BSA and glycerol, respectively [15]. However, the amount of BSA was not same as the protocol followed in the paper 'Multilayered tissue-mimicking skin and vessel phantoms with tunable mechanical, optical, and acoustic properties' [15]. Here, 3g of gelatin powder was dissolved in 30ml of DI water along with 1.5ml (calculated as 5% of the 87% stock solution) of glycerol. That solution was kept on a magnetic hot plate at 230°C with continuous stirring. After a while, the solution started to boil, and it took about 11 minutes to mix properly. Half of the solution (almost 15ml) was poured into a 1cm thick and 5.3cm wide circular petri dish. In the other half of the solution, 0.05% or 150µl of glutaraldehyde of the stock solution (5% glutaraldehyde in PBS) was added at approximately 58.8°C. Then the solution was transferred to another petri dish.

In the dermis layer, the attenuation coefficient and the speed of sound are dominated by collagen/elastin, which can be achieved by using BSA and methanol, respectively [15]. 12% of gelatin and 0.5% of agar powder were dissolved in two different beakers; each

carried 20ml of DI water. The amount of gelatin seemed relatively high compared to water. Afterward, both the solutions were transferred into one beaker, and it was placed on the hot plate at 290°C. Since the percentage of gelatin was relatively high in this solution, it took about 25 minutes to dissolve completely. However, the solution wasn't completely transparent; it carried some coagulated gelatin in it. Later the solution was cooled down to 30°C to add 4.25% or 1.7g of lyophilized or freeze-dry BSA powder under continuous stirring with a magnetic stirrer. The denaturing temperature of BSA is below 30°C; thus, it was added slowly to the solution at that temperature [15]. Half of the solution was poured into a similar type of petri dish before adding methanol; later, 15.31% or 6.124ml of methanol was added to the solution and poured into another petri dish.

In the hypodermis layer, the acoustic properties are dominated by adipose in human tissue. Similar to the dermis, these properties can be replicated in phantom hypodermis by using BSA and methanol. The process of preparing the phantom hypodermis layer is similar to the dermis layer. The difference here is the changing amount of different chemicals. In a beaker, 0.3g or 2% of gelatin powder and 0.03g or 0.2% of agar powder were dissolved in 15ml of DI water at room temperature. Since the percentage of powder is low compared to the dermis layer, it was easy to dissolve into water. Then, the beaker was placed on a hotplate with continuous stirring with a magnetic stirrer at 290°C for about 19 minutes. 3.33% or 0.5g lyophilized BSA was added to the solution at 30°C. Half of the solution was poured into a petri dish in the same way to the dermis before adding methanol; 23.45% or 7.035ml of methanol was added to the other half solution and later transferred into another petri dish. All the solutions were kept at room temperature for 24 hours to set in the petri dish properly, which is shown in figure 9. The chemical composition for phantom preparation is given in table 5.

The percentage amount for all the chemicals could not be followed with the mentioned protocol [15] because of the shortage of chemicals. Therefore, the calculated amount of chemicals was low compared to the protocol, and modification can be done in amount to see the changes in properties. However, due to the time limit, this could not be investigated.



Figure 9: Different phantom gel layers in petry dishes

Table 5: Chemical composition of phantom skin layers to obtain the target acoustic properties in the lab

Chemicals	Epidermis		Dermis		Hypodermis	
	Percentage (%)	Amount in grams or milliliters	Percentage (%)	Amount in grams or milliliters	Percentage (%)	Amount in grams or milliliters
DI water	-	30	-	40	-	15
Gelatin	10	3	12	4.8	2	0.3
Agar	-	-	0.5	0.2	0.2	0.03
Glycerol (87% stock)	5	1.5	-	-	-	-
Glutaraldehyde (5% in PBS)	0.05	0.15	-	-	-	-
BSA	-	-	4.25	1.7	3.33	0.5
Methanol	-	-	15.31	6.124	23.45	7.035

4.3.2 Fabrication of homogeneous phantom skin

In this experiment, homogeneous phantoms were prepared to replicate the attenuation coefficient and speed of sound of human skin by following the paper 'Tissue-mimicking

phantoms for photoacoustic and ultrasonic imaging' by Jason R. Cook, Richard R. Bouchard, and Stanislav Y. Emelianov. Six phantom skins were prepared with varying concentrations of chemicals mentioned in table 6. The whole experiment was conducted inside the fume hood in Zimmer & Peacock cleanroom. The amount of DI water and formaldehyde were similar for all, which is 15ml and 0.1% or 45.54 μ l (37% formaldehyde stock solution). The variable element for the chemical preparations was gelatin, which was 4%, 6%, 8%, 10%, and 12% or 0.6g, 0.9g, 1.2g, 1.5g, and 1.8g, respectively. An additional gelatin solution was prepared with 10% gelatin powder to see the difference in acoustic properties between the plain gelatin gel and the gel with formaldehyde.

Table 6: Amount of different chemical for agar gel preparation

Sample	DI water (ml)	Gelatin (%)	Formaldehyde (%)
1	15	4	0.1
2	15	6	0.1
3	15	8	0.1
4	15	10	0.1
5	15	12	0.1
6	15	10	-

A beaker carrying 15ml of DI water was placed on a hot plate with a magnetic stirrer in it. The temperature was recorded with a thermometer. At 30°C, formaldehyde was added to the water, and around 50°C temperature, the measured gelatin powder was added slowly to dissolve properly. Formaldehyde helps to increase the cross-linking of the phantom gel [16]. The solution was heated for 10 minutes with a lid on top of the beaker displayed in figure 10. The cover helped to mitigate the vapor loss. Afterward, all the solutions with different amounts of chemicals mentioned in table 6 were prepared and transferred to petri dishes and kept at 4°C temperature to form gels.



Figure 10: Phantom skin sample on the hotplate (turned on) covered with a lid to avoid evaporation of the chemical solution

4.4 Setup for the characterization of acoustic properties of phantom skin

For the characterization, many researchers used two single elements or one ultrasound transducer in Megahertz (MHz) range frequencies by placing the specimen underwater [14]–[16], [25], [42]. These papers mainly referred to the University of Wisconsin laboratory's transmission method [24]. The whole process for the characterization is shown in figure 11.

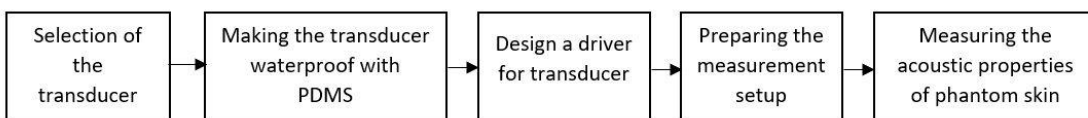


Figure 11: Characterization of phantom skin model

4.4.1 Selection of the transducer

Most of the researchers achieved success in replicating similar acoustic properties of human skin with the transducer in the MHz range. Therefore, a piezoelectric ceramic disc with a 16mm diameter, 1.5mm thickness, and 1 MHz frequency was selected, shown in figure 12. The characterization experiment required two similar transducers, one as a

transmitter and another as the receiver. The piezoelectric transducer needs to be insulated before transmitting any signal inside water.

4.4.2 Insulation with polydimethylsiloxane (PDMS)

PDMS is popular in the biomedical industry for its comparable biocompatible and biomechanical behavior as biological tissue, and it is a polymer of silicone elastomer group [43]. Among its numerous usages, PDMS can be used as an insulation and hydrophobic layer for any conductive material [24], [44].

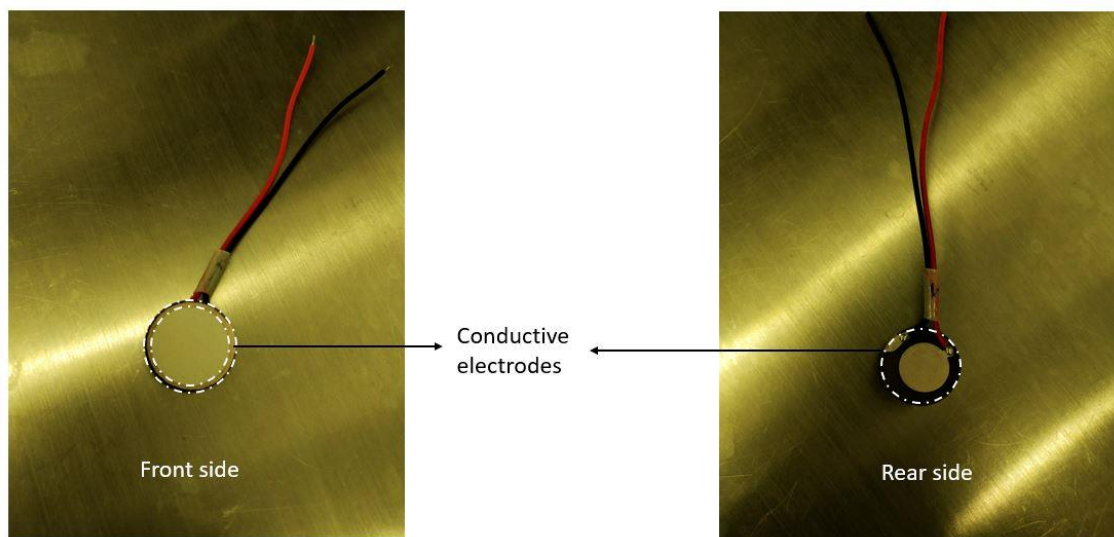


Figure 12: Front and rear sides of the piezoelectric transducer

The piezoelectric transducer selected for the experiment is conductive because of the electrodes and any exposed piezoelectric area, which have metal layers shown in figure 12. The transducer has a silicone cover shown in figure 13, and this cover makes the front side non-conductive as the front side has conductive metal only on the edge of the circle. On the other hand, the rear side of the transducer is entirely conductive.



Figure 13: Piezoelectric transducer with silicone cover

A thin layer of PDMS on the conductive part of the transducer was applied. At first, the PDMS solution was prepared. It has two parts of polymer- silicone elastomer base and curing agent. The ratio of silicone elastomer base and curing agent is 10:1 [45]. In this case, the measured amount for elastomer base and curing agent was 10.033g and 1.041g, respectively. Then the solution was mixed homogeneously in the speed mixer at 2500rpm for 4 minutes. The first applied method for PDMS coating was to dip the transducers into the solution and dry it for two days. Afterward, the resistance of the transducer's conductive part was measured with a multimeter, and it showed some resistance. Later a more repetitive method was tried for the PDMS coating of the transducers. The major conductive part of the transducer is the rear part, and it has no participation in sending or receiving signals for the characterization experiment. Therefore, approximately 200g of PDMS solution was poured on the transducer's rear part, and it was placed on the spinner machine in the cleanroom. The device's spinning program was acceleration time for 30 seconds, spinning at 200rpm for 30 seconds, and deceleration time for 30 seconds. Later both the transducers were baked at 65°C for 2 hours.

4.4.3 The resonance frequency of the transducer

At the resonance frequency, the transducer transmits or receives maximum signal/energy. Therefore, it is essential to determine the resonance frequency before the experiment to send the optimal signal. It is easy to decide on the resonance frequency from an impedance graph, shown in figure 14 [46]. The minimum impedance frequency is the resonance frequency, and the maximum impedance frequency is the anti-resonance frequency. The transducer's resonance frequency was measured in the ultrasound lab with the network analyzer device displayed in figure 15. The measurement of the resonance frequency before and after insulation can help figure out any frequency alteration.

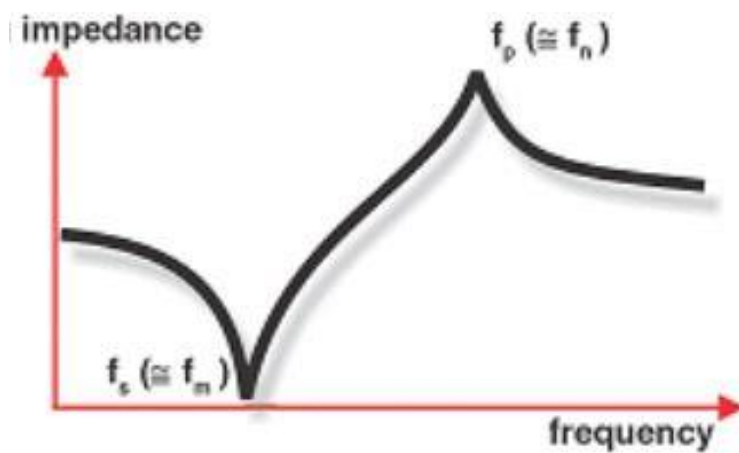


Figure 14: Impedance Vs. frequency graph (f_s is the resonance frequency & f_p is the anti-resonance frequency) [46]

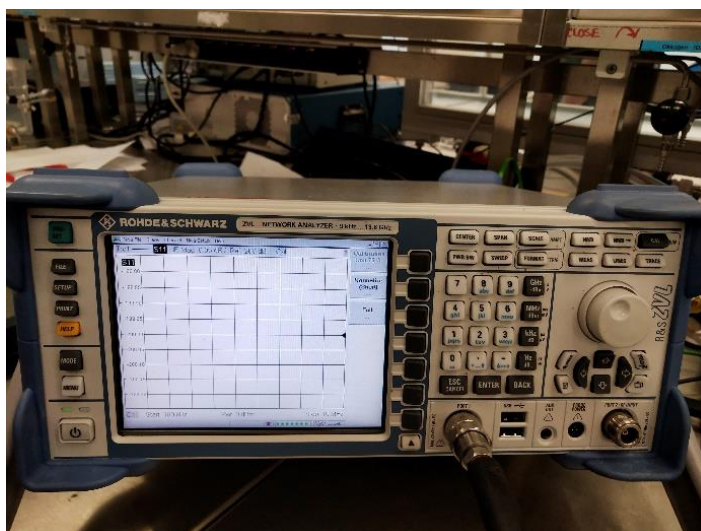


Figure 15: Network analyzer for impedance measurement

4.4.4 Driver for ultrasound transducer

A PCB model was designed for the driver, and it was fabricated in the electronics lab. CD 4007UBE is preferable for the driver design, which has 9 MOSFETs integrated inside the integrated circuit (IC). The circuit diagram of CD 4007UBE is given in figure 16. This IC supplies high current, and it's easy to create a digital inverter with it. The circuit design for the driver is shown in figure 17.

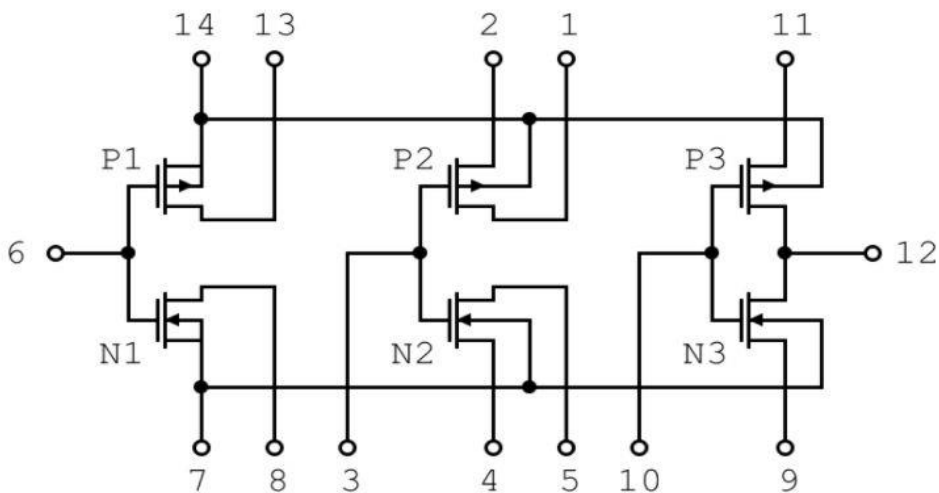


Figure 16: Circuit diagram of CD 4007UBE [58]

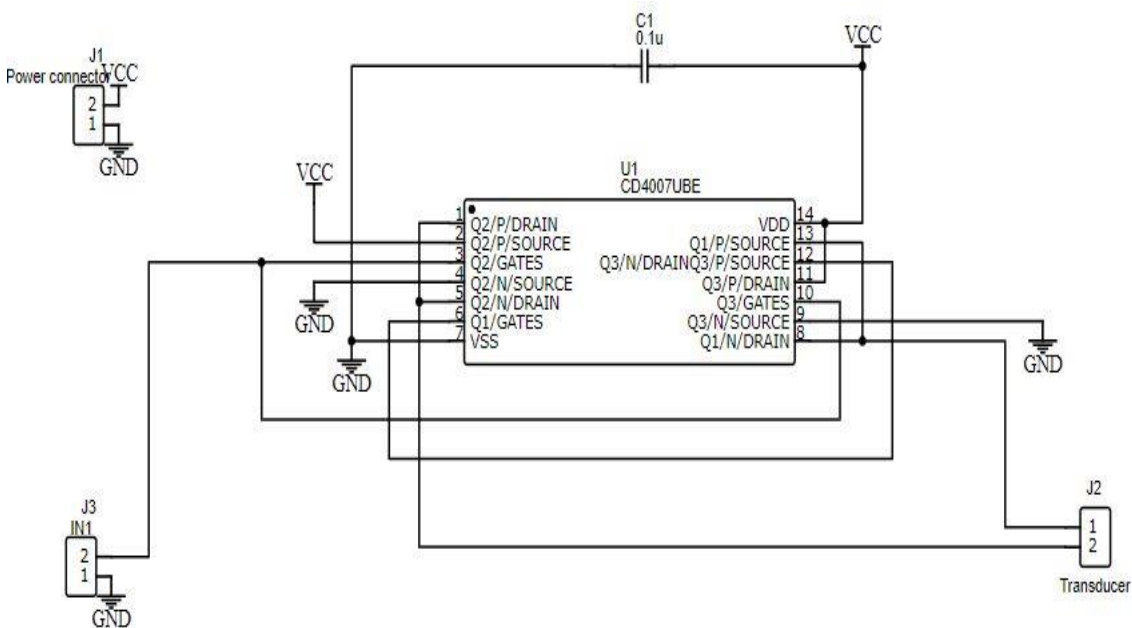


Figure 17: Circuit design for the driver

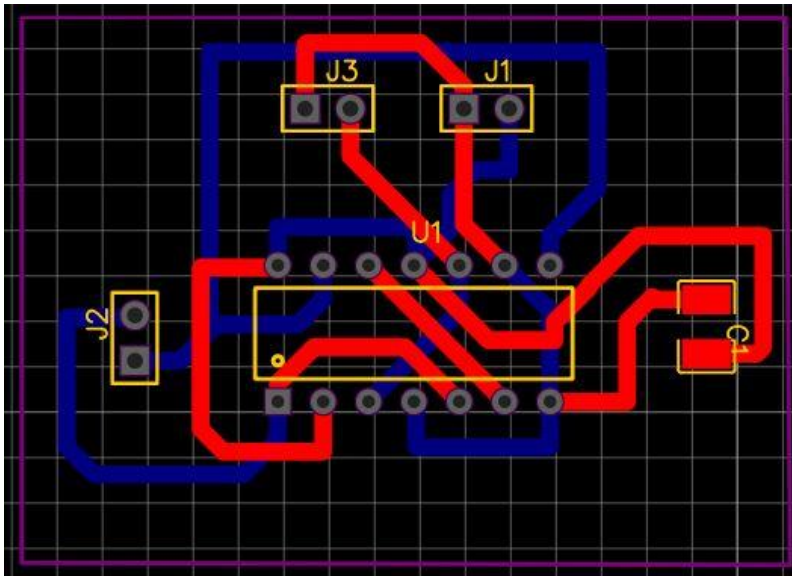


Figure 18: PCB layout of the driver

The PCB design layout shown in figure 18 was printed, and it was fabricated on a PCB board. Later all the components were soldered on the board in the electronics lab.

4.4.5 Measurement of acoustic properties

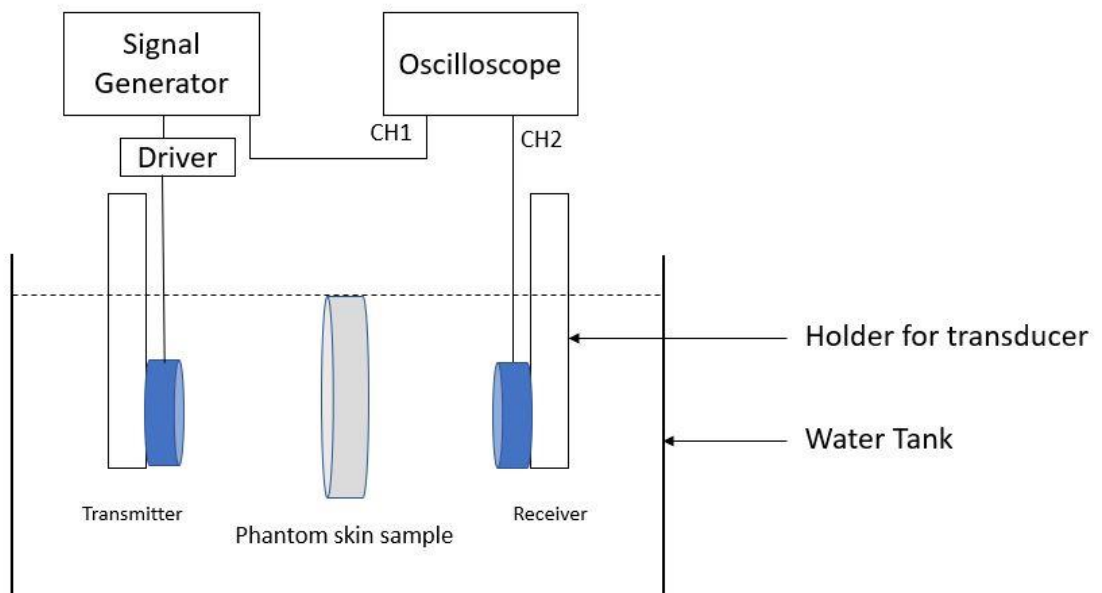
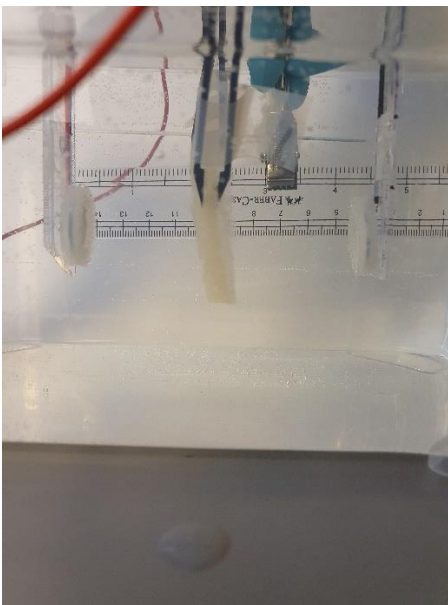


Figure 19: Schematic of the experimental setup for the acoustic measurement

The experimental setup for this measurement was followed in the same way of figure 19. Both the transducers were placed inside the water parallelly without touching the tank's bottom, and the distance between the transducers, which is known as the beam path, was approximately 9cm (± 1 mm), shown in figure 20a. Each sample from the layered phantom method was mounted in the middle simultaneously, trying to have an equal distance from the transducers. All the samples were extracted very carefully with a metal spatula shown in figure 20b. However, it wasn't easy to place the sample precisely in the middle because it had a curvature in its shape while putting it inside the water tank.



(a)



(b)

Figure 20: (a) Phantom sample in the beam path; (b) Extraction of the sample with a metal spatula

The transmitting transducer was connected to a signal generator. Both the transmitter and receiver transducers were connected to an oscilloscope to observe the signals. The operating frequency for the transducers was 1.94MHz. The signal generator supplied ten cycles of sinusoidal signal with a 2ms burst period and 10V amplitude during measurement. Here, a 2ms burst signal was chosen so that the time is sufficiently large before sending a new burst, which can help to ensure that both the transmitted and received signals are in equilibrium before sending a new burst. Ten cycles of sinusoidal wave signal with 10V amplitude were selected by following the protocol mentioned in 'Tissue-mimicking bladder wall phantoms for evaluating acoustic radiation force—optical

coherence elastography systems' by O'tega A. Ejofodomi, Vesna Zderic, and Jason M. Zara. Afterward, the signals were recorded without the sample and with the sample inside the water tank. Both the SOS and the attenuation can be calculated from these signals. Later homogeneous phantom skins were fabricated for a similar experiment. The insulation failed at that time; that's why the experiment could not be performed.

The speed of sound in water (C_W) can be calculated from equation (5),

$$C_W = \frac{\text{Space}}{\text{Time}} \quad (5)$$

For the measurement setup presented in figure 19, each phantom skin's speed of sound can be calculated using equation (6) [25].

$$C_P = \frac{d_P}{T - T_W \frac{d - d_P}{d}} \quad (6)$$

Here, C_P is the speed of sound, d is the distance between transmitting and receiving transducer, T and T_W are the time of flights when the sample is present and absent inside the water tank, d_P is the thickness of the sample.

Equation (7) is appropriate to calculate the phantom skin's attenuation coefficient calculation for the established setup in this experiment [25].

$$\alpha_P = \frac{\ln \frac{V_W}{V}}{d_P} \alpha_W \quad (7)$$

Here, α_P is the attenuation coefficient, V_W and V are the amplitudes of received signals when the samples are absent and present inside the water tank, d_P is the thickness of the sample and α_W is the attenuation of water at room temperature that can be calculated from equation (8) [47], [48]. The unit for attenuation is Neper per centimeter (Np/cm) or decibel per centimeter (dB/cm).

$$\alpha_W = 0.0002f^2 \quad (8)$$

Here, f is the frequency of the transducer, and 1 Np = 8.686 dB.

5 Materials

5.1 Consumables

Sodium chloride (S3014, Sigma Aldrich, Norway)

Bovine serum albumin (A9418 or 05470, Sigma Aldrich, Norway) (Merch, Darmstadt, Germany)

Formaldehyde (252549, Sigma Aldrich, Norway)

Polydimethylsiloxane (SYLGARD™ 184 base and curing agent, Dow Chemical Company Limited, Derbyshire, England)

Glutaraldehyde (340855 or G7651, Sigma Aldrich, Norway)

Glycerol (VWR, Norway)

Gelatin powder (48723, Sigma Aldrich, Norway)

Agar powder (A7002, Sigma Aldrich, Norway)

Methanol (VWR, Oslo, Norway)

Deionized water

5.2 Tools and devices

Piezoelectric ceramic disc- H4P81000

Conductivity meter (RS, 1410-1002)

Signal Generator (Tektronix, AFG1062)

Oscilloscope (Keysight, DSOX3024T)

Speed mixer (Synergy devices limited, DAC 150FVZ-K)

Network Analyzer (ROHDE & SCHWARZ)

Spinner 2 AB plast Soin 150

Multimeter (KEITHLEY, DMM6500)

Power source

Pipettes

Magnetic hotplate

Thermometer

6 Results and discussion

6.1 The conductivity of phantom skin

The conductivity of the phantom skin was measured with two instruments, shown in figure 7 and figure 8. The measurement results are reported in table 7 and table 8, respectively.

Table 7: Measured conductivity with the multimeter (DMM6500) of different solutions

Sample	Molarity	Conductivity of NaCl solution at room temperature (mS/cm)	Conductivity of NaCl + agar gel (mS/cm) at room temperature
1	342mM	0.0069	0.0068
2	171mM	0.0074	0.0065
3	85mM	0.0072	0.0064
4	42mM	0.0070	0.0062

Table 8: Measured conductivity with the conductivity meter (1410-1002) of different NaCl concentration with agar gel solutions

Sample	Molarity	Conductivity of NaCl solution at room temperature (mS/cm)	Conductivity of 13 ml NaCl + 13.5ml agar gel at 20°C (mS/cm)	Conductivity of 20 ml NaCl + 13.5ml agar gel at 50°C (mS/cm)
1	342mM	24.9	14.14	16.1
2	171mM	12.74	7.46	9.89
3	85mM	6.93	4.1	4.91
4	42mM	3.45	2.53	2.74

The recorded results from table 7 are pretty low compared to the expected data and the recorded data with the conductivity meter probe. The probable reason could be that the probes for measuring the resistance are not compatible with liquid or semi-liquid material. It is also challenging to keep a steady distance between the probes for accurate

measurement. It was verified from the measured values of table 8, which displays that the conductivity meter probe measured the conductivity in the same range of expected values. However, the values have reduced almost half from the desired results. This reduction in conductivity could be due to using a different amount of NaCl than the followed protocol [41]. To see any change in conductivity, an extra 20ml of NaCl was added in a similar process. The recorded data is confirmation for increasing conductivity with an increase with the electrolyte (NaCl) inside the solution up to a particular concentration, which is related to the solubility of the chemical [49]. However, the solution's temperature was higher than the other solution, which consisted of 13ml of NaCl solution. It also can be another factor for some increase in conductivity [49].

Figure 21 has compared the conductivities of different molarity solutions of NaCl solution, 13ml of NaCl and agar powder solution, and 20ml of NaCl and agar powder solution. The conductivity increases with NaCl concentration. It also increases with the amount of NaCl in the agar solution. However, the agar gel is breakable if the liquid solution of NaCl is increased too much. Keeping this in mind, the experiment can be repeated with higher concentrations of NaCl solution, and any cross-linker can be used to have better strength. The conductivity is likely to be raised with the rising concentration of NaCl. After mixing the NaCl solution with agar solution, the conductivity seemed to be decreased. This decrease in conductivity is because of the increasing amount of DI water in the solution. Figure 22 displays the comparison of the same molarity NaCl with the varying amount of NaCl and agar solution. It can be concluded that the amount of NaCl helps to increase conductivity. However, the solubility of NaCl in water should also be considered, which is 357mg/ml at 25°C [50].

From the recorded data of table 8, it can be concluded that the agar gel with 13ml of 171mMol NaCl has comparable conductivity with human dry skin (0.68956 S/m or 6.8956 mS/cm) [32]. Therefore, this recipe can be used to fabricate phantom skin with similar electrical properties to human skin.

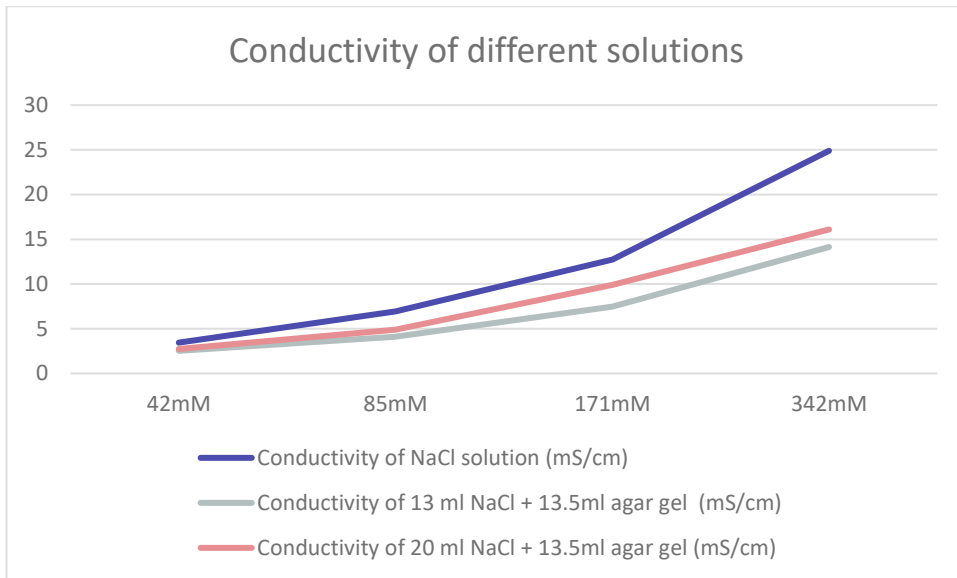


Figure 21: Change in the conductivity with varying concentrations of NaCl

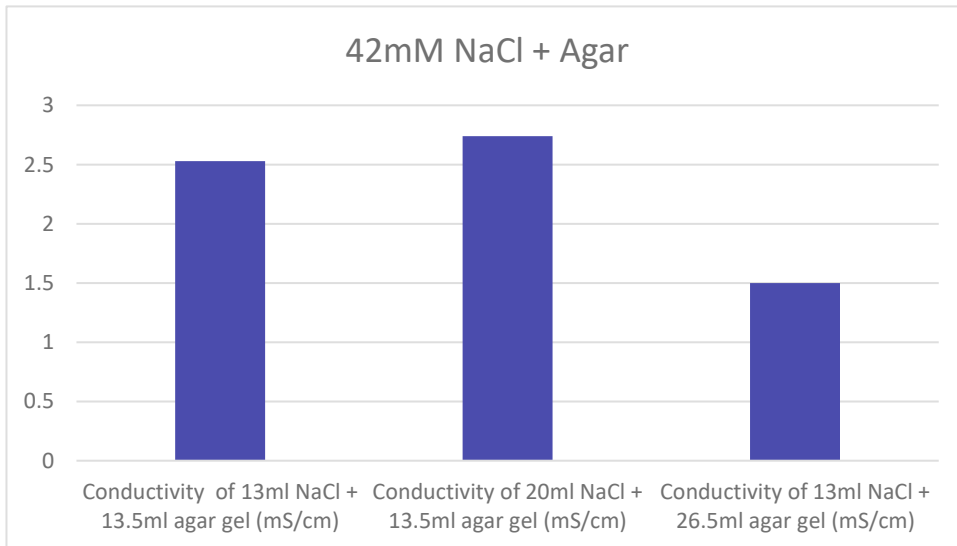


Figure 22: The conductivity comparison with varying amounts of NaCl solution

6.2 Resonance frequency

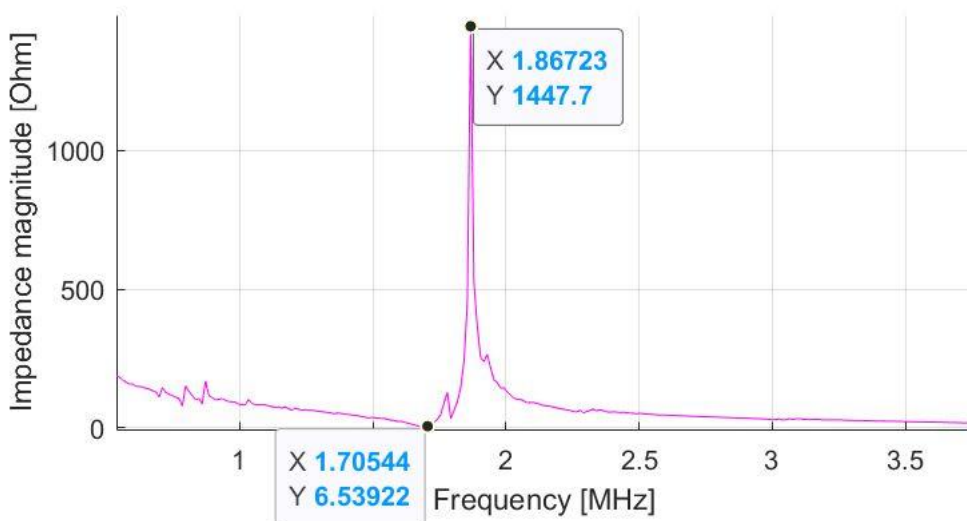
The transducer's resonance frequency was determined from the impedance graphs illustrated in figure 23. There is a slight deviation in both transducer's resonance frequencies after applying PDMS on it. The resonance frequencies for the transmitter and receiver transducer before insulation were 1.70544MHz and 1.74278MHz, respectively. After the insulation with PDMS and the silicone cover on it, the frequencies are 1.69300MHz and 1.70544MHz, respectively. The deviation in the resonance frequency of

the transmitter and receiver are 12.44KHz and 37.34KHz. Therefore, the shift in resonance frequencies is relatively low after applying PDMS on the transducers.

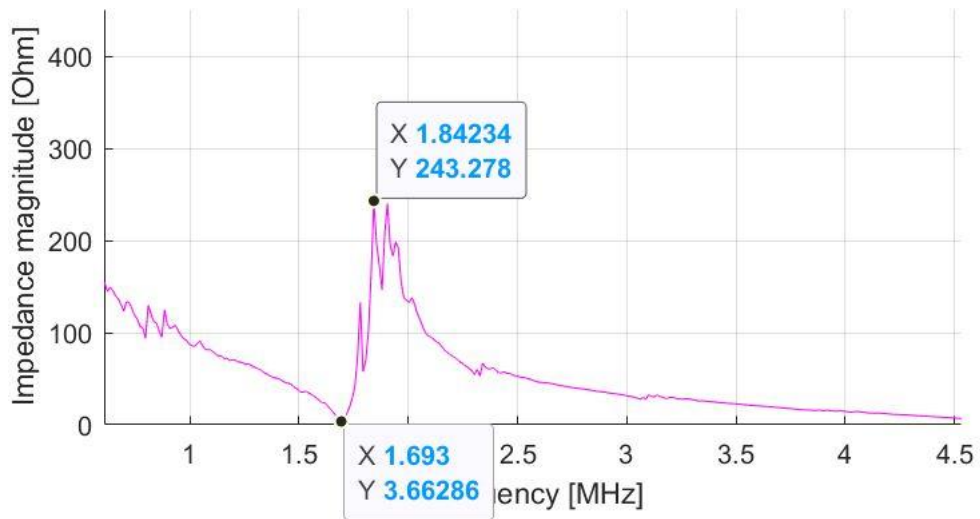
Table 9: Resonance frequency of the transducers

Transducer	Resonance before PDMS (MHz)	Resonance after PDMS (MHz)
Transmitter	1.70544	1.69300
Receiver	1.74278	1.70544

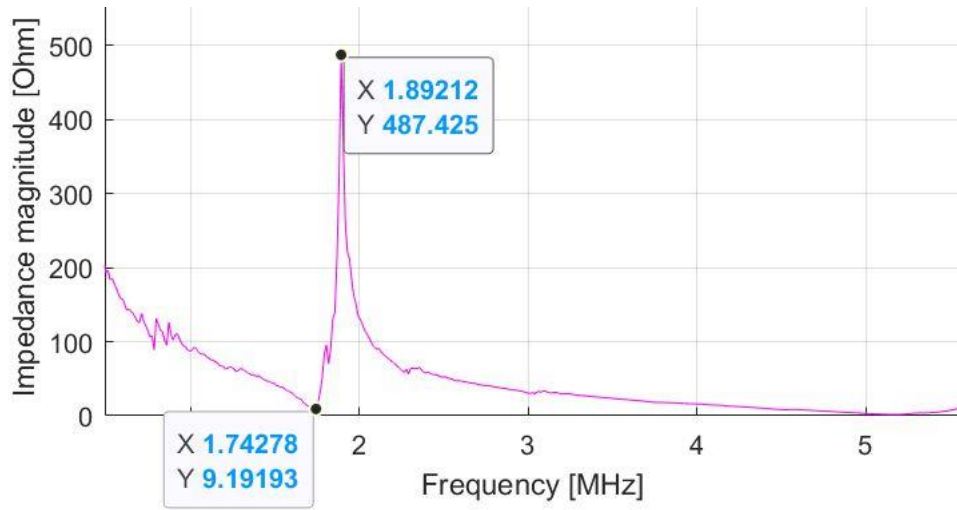
From the result mentioned in table 9, it is established for this experiment that the transducers' rear side insulation affected the resonance frequencies approximately 0.73% to 2.18%. The resonance frequency depends on some factors such as stiffness, mass, etc. The PDMS process was manual; therefore, the applied amount for both the transducers was not similar. This can be a reason for the difference in frequency shifts as resonance frequency depends on mass.



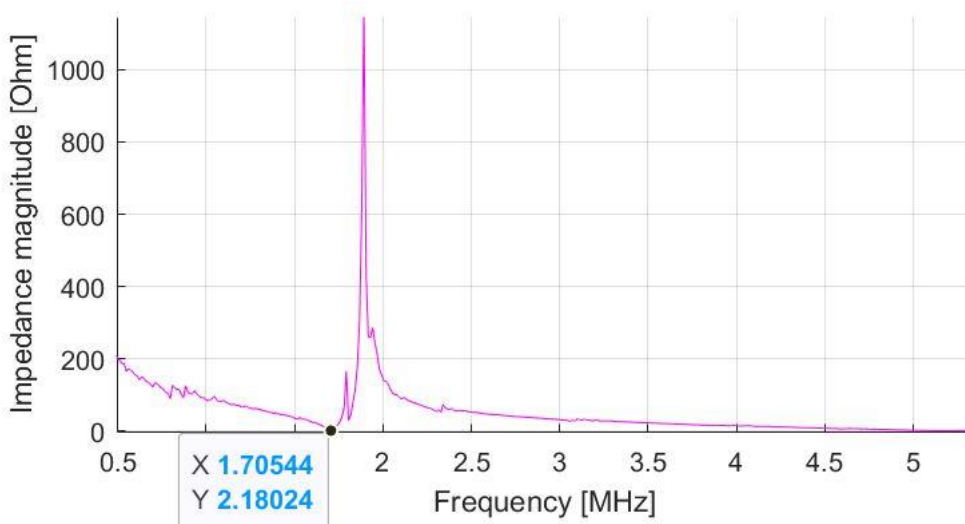
(a)



(b)



(c)



(d)

Figure 23: (a) Transmitter's resonance frequency before PDMS, (b) Transmitter's resonance frequency after PDMS, (c) Receiver's resonance frequency before PDMS, (d) Receiver's resonance frequency after PDMS

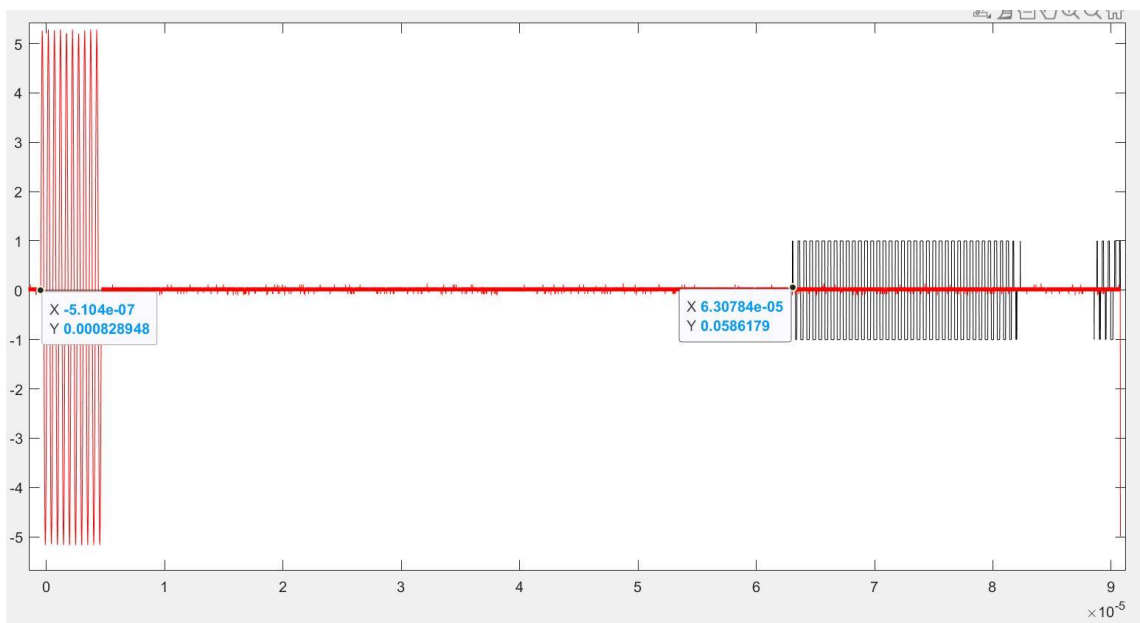
The operating frequency for the transducer was chosen 1.94MHz mentioned in the method section instead of the resonance frequency. In this case, this is the best transmitting frequency for the transducer, probably because the impedance of the transducer is equal to the complex conjugate impedance of the driver at this frequency. The driver output impedance is unknown here. Therefore, the reason for getting the best transmission at 1.94MHz could be the impedance of the driver matches with the impedance of the transducer at this frequency.

6.3 Speed of sound (SOS) of phantom skin

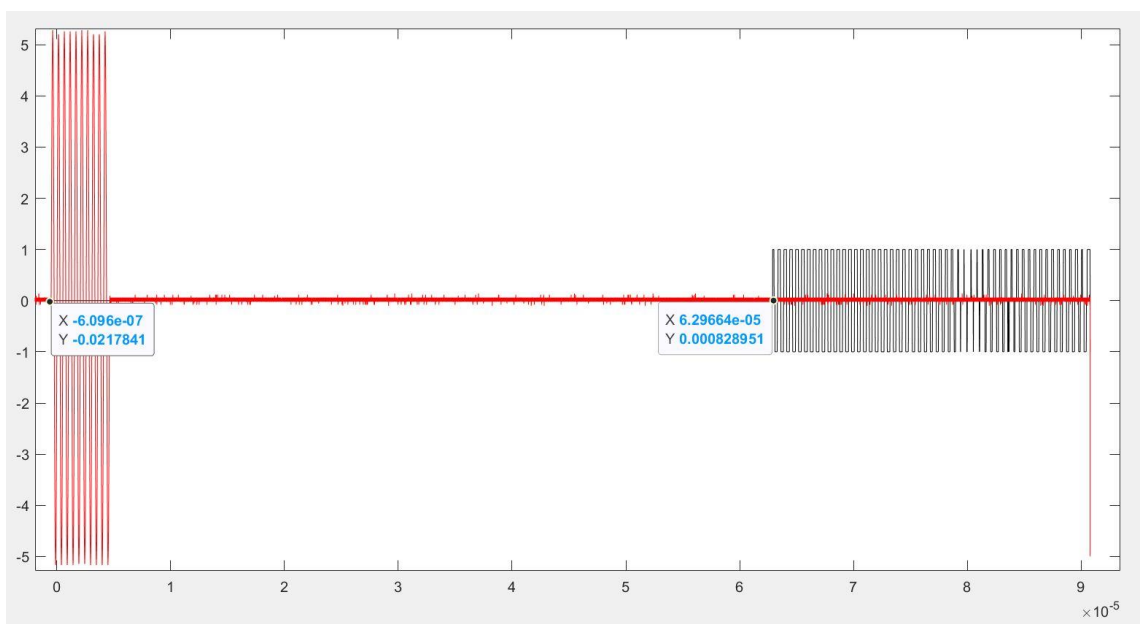
The speed of sound was measured with the transducer setup mentioned in the method section, displayed in figure 20a. The calculated results from the oscilloscope graphs without sample, with samples such as epidermis with glutaraldehyde, dermis with methanol, and dermis without methanol, are shown in figure 24. Other layers of phantom skins were breakable in water; thus, it was not possible to record the measurement for those layers. First, the speed of sound in the air was calculated to validate the measurement setup, and it was about 339ms^{-1} , which is almost equal to the established value 343ms^{-1} [52]. The signal generator supplied ten cycles of sinusoidal signal with a

2ms burst period and 10V amplitude during measurement, and the transducer's operating frequency was 1.94MHz.

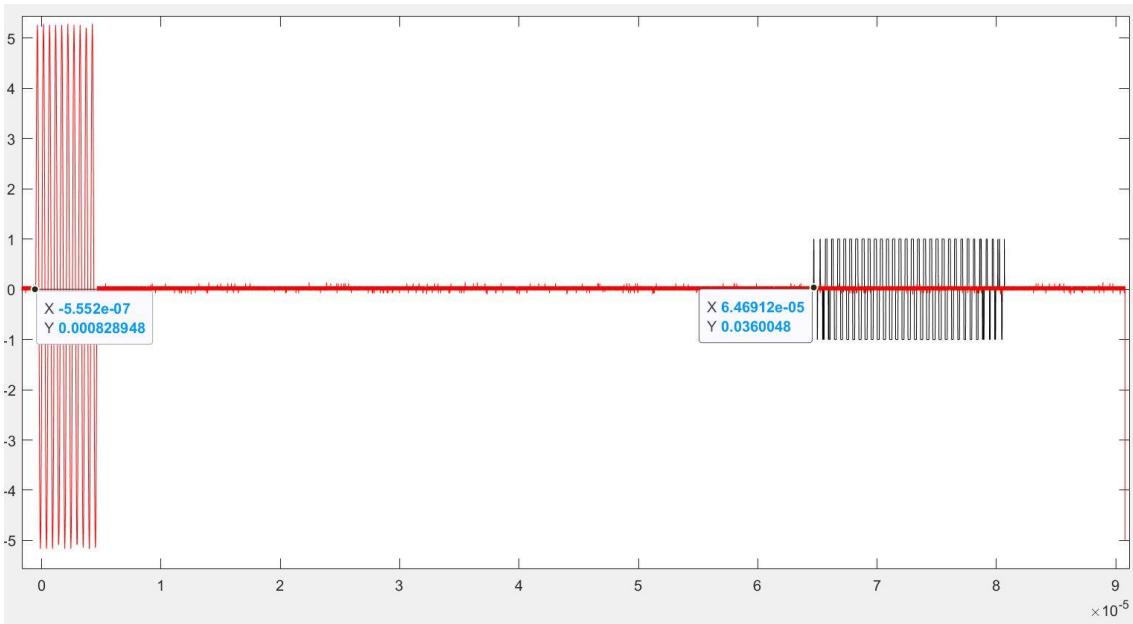
Figures 24 and figure 25 (displayed in the next section) represent the same signals. Only the data of figure 24 was post-processed with MATLAB simulation to identify the starting of the received signals for SOS calculation. Therefore, signals in figure 25 have more noise compared to figure 24.



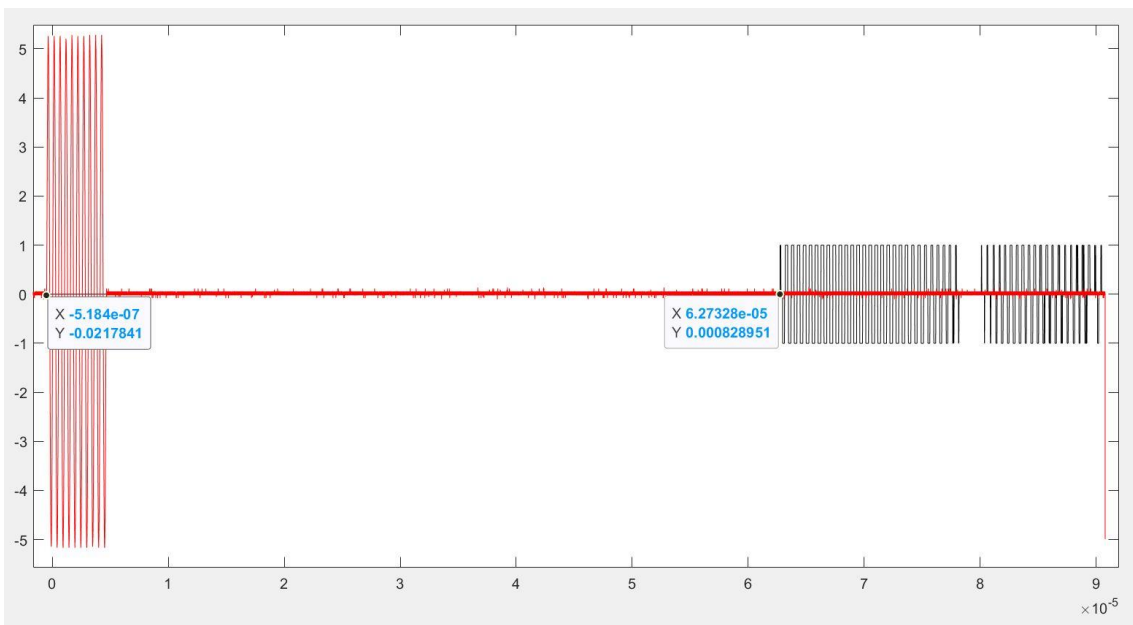
(a)



(b)



(c)



(d)

Figure 24: (a) Transmitted & received signals in the water, (b) Transmitted & received signals for epidermis with glutaraldehyde, (c) Transmitted & received signals for dermis without methanol, (d) Transmitted & received signals for dermis with methanol

The time flights with and without samples in the experiment were measured by calculating the transmitting and receiving signal's start point shown in figure 24. Table 10 illustrates the speed of sound in water, dermis layer with and without methanol, and

epidermis with glutaraldehyde in it. The SOS calculation has been done by following the equations (5) and (6) given in the method section.

Table 10: Speed of sound of the phantom samples

Data	Dermis without methanol	Dermis with methanol	Epidermis with glutaraldehyde
D (cm)	9	9	9
T (μ s)	0.652	0.633	0.635
T _w (μ s)	0.636	0.636	0.636
Time delay (μ s)	0.016	0.003	0.001
D _p (cm)	0.8	0.8	0.8
C _p (ms ⁻¹)	1102.9	1494.4	1440.6

The SOS in water at 20°C is 1481.8ms⁻¹ [53]. The calculated SOS in water for the experiment is 1415.1ms⁻¹ with a 9cm distance between the transducers. The temperature of the water was approximately 20°C. Therefore, the calculated value is 66.7ms⁻¹ or 4.5% lower compared to the expected value. The reason for this deviation can be the slightly deviated alignment of the transducers.

In phantom materials, SOS should increase linearly with the rising concentration of gelatin, agar, and BSA in the solution. And methanol helps decrease the SOS by 3.77ms⁻¹ with an increase of each percent; however, other literature described that alcohol increases the SOS [15], [23]. The calculated SOS from table 10 for the dermis without methanol, dermis with methanol, and epidermis with glutaraldehyde are 1102.9, 1494.4, and 1440.6ms⁻¹, respectively. The SOS in the human dermis is about 1595ms⁻¹, and the average SOS in soft tissue is 1540 ms⁻¹ [15], [16]. Therefore, the results are low compared to established values, such as the dermis layer with methanol is 100.6ms⁻¹ or 6.3% lower than 1595 ms⁻¹, and the epidermis layer is 99.4ms⁻¹ or 6.45% lower than 1540 ms⁻¹. The percentages of chemicals were significantly less. Especially in dermis layers, the amount of BSA was low compared to the method followed for this experiment [15]. Other reasons can be the proper alignment problem of the transducer, and the sample also had a curvature during measurement.

Moreover, the samples were not completely clear as a solution, especially the dermis phantom without methanol had a considerable amount of bubbles and sediments. It is easier for a signal to pass through a sample if it is homogeneous. The SOS in the dermis layer with methanol is lower than the layer without methanol from the results. Therefore, the methanol increased the SOS instead of decreasing it, or the bubble layer at the top of the sample without methanol troubled the transmitting signal. Hence, the results are different than the followed protocol [15].

Table 11: Time delay calculations from different papers

Sample thickness (cm)	SOS with sample (ms^{-1})	SOS in water (ms^{-1})	Time of flight with sample (μs)	Time of flight without sample (μs)	Time delay (μs)	References
3.85	1499.356	1501.34	25.68	25.64	0.04	[17]
5	1561	1489 (at 22°C) [53]	32.03	33.58	1.55	[24]
2.3	1593	1494 (at 26°C) [53]	14.44	15.39	0.95	[54]

Table 11 displays the time delay calculations from different papers with different thicknesses of the specimens, and the ambient temperature is also a variable for these experiments. The time delays for sample thicknesses of 3.85, 5, and 2.3cm are 0.04, 1.55, and 0.95 μs , respectively. The mentioned time delays are higher than the time delays found in this experiment which are 0.001, 0.003, and 0.016 μs for different samples with small thicknesses (0.8cm), given in table 10. To improve the reliability of our measurement, the thickness of the samples should be larger. Here, an oscilloscope is used to measure the time delay, and every oscilloscope has a minimum resolution it can measure. If the time delay of the fabricated phantom samples is smaller than the minimum resolution of the oscilloscope (measurement tool), it is difficult to understand the time delay. In this measurement, the main source of error was the time delay

measurement; thus, the calculated values do not match the theory. Therefore, making the phantom samples thicker would improve the results.

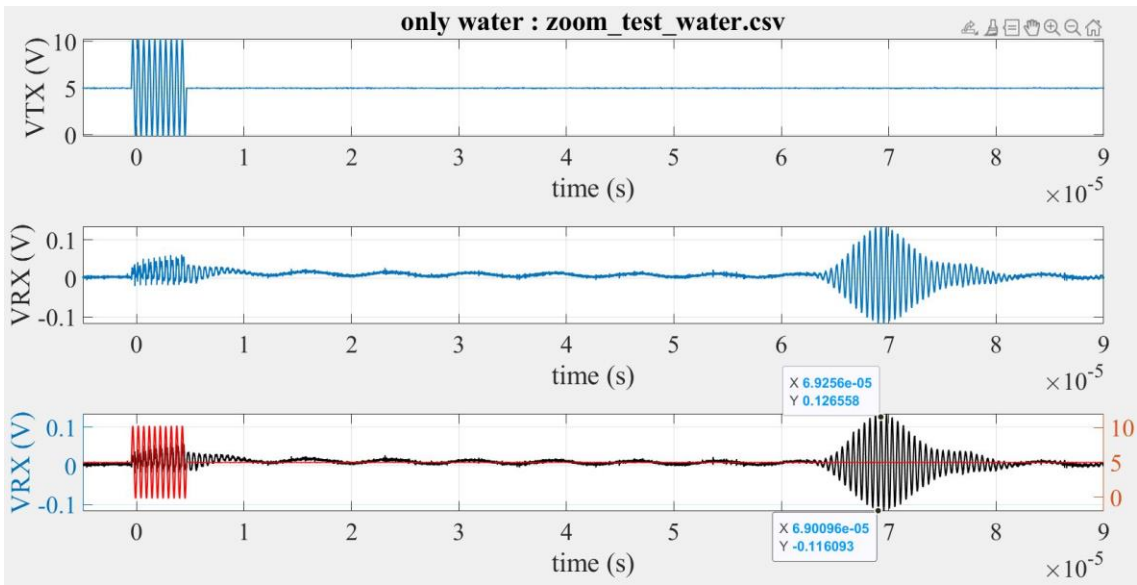
6.4 Attenuation coefficient of phantom skin

The attenuation coefficient was calculated with the same transducer setup and signals, shown in figure 20a. In calculating the attenuation coefficients, the amplitudes of received signals were measured, displayed in figure 25. The attenuation coefficients for the different phantom samples have been calculated from equation (7) given in the method section, and the calculated values are displayed in table 12.

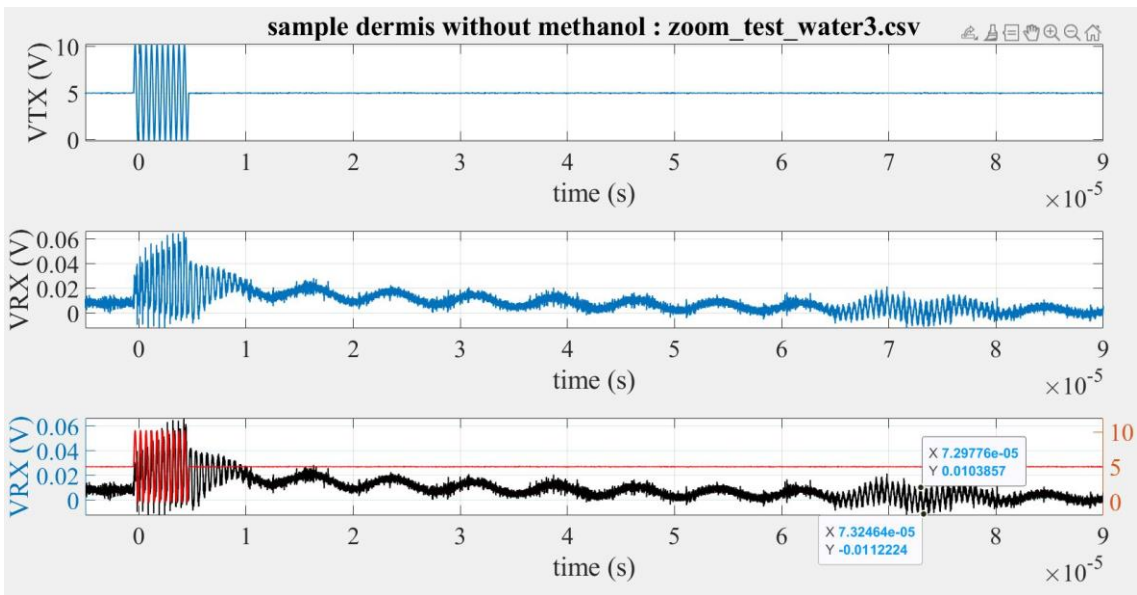
For the selected transducer, the applied frequency was 1.94MHz. Therefore, the attenuation coefficient for water in this frequency domain is 0.000753Np/cm or 0.00653dB/cm, calculated from equation (8) given in the method section.

Table 12: Attenuation coefficient of different samples

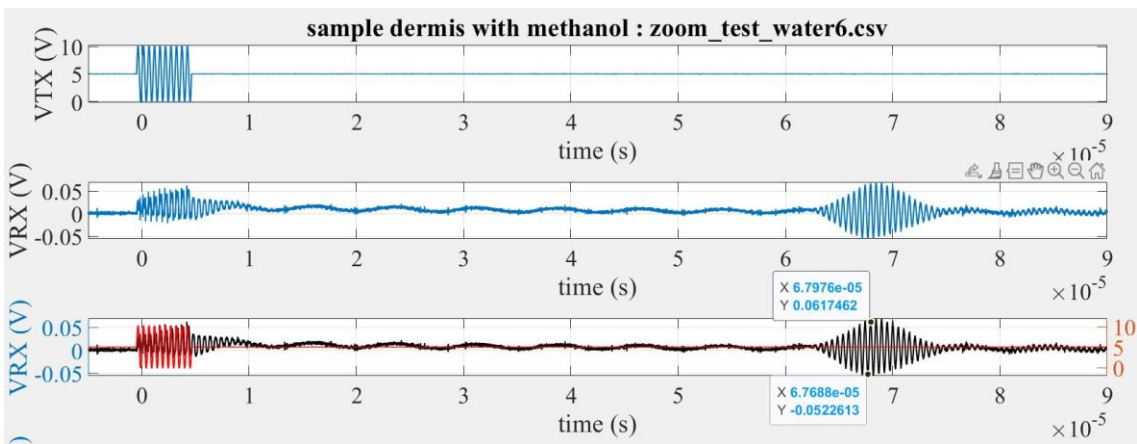
Data	Dermis without methanol	Dermis with methanol	Epidermis with glutaraldehyde
α_W (dB/cm)	0.00653	0.00653	0.00653
V (V)	0.02	0.11	0.15
V_w (V)	0.23	0.23	0.23
D_p (cm)	0.8	0.8	0.8
α_P (dB/cm)	0.019	0.006	0.003



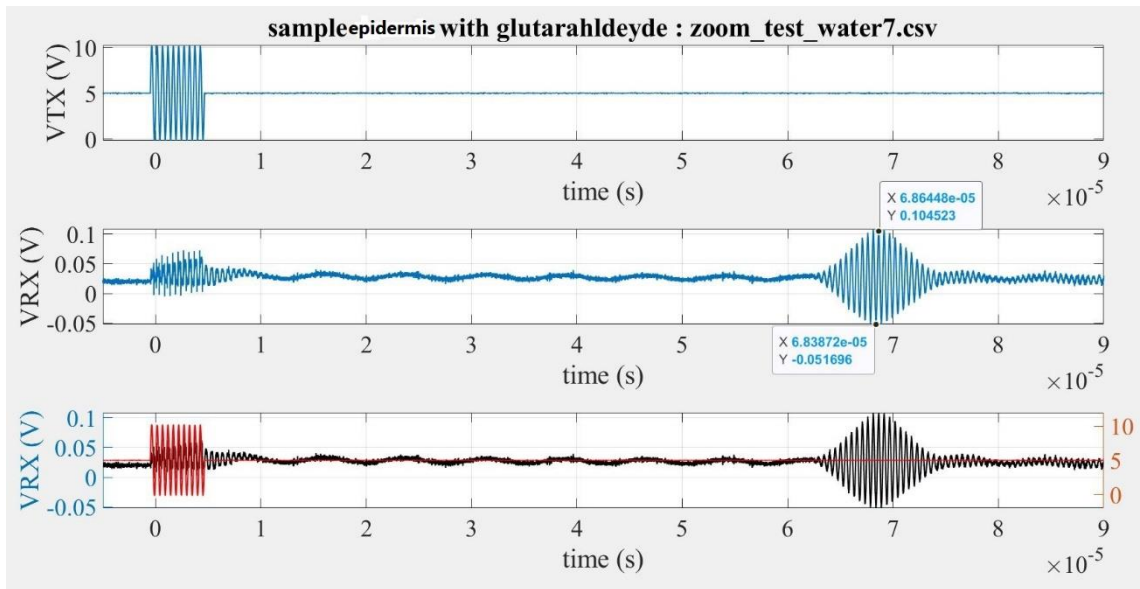
(a)



(b)



(c)



(d)

Figure 25: (a) Transmitted & received signals in the water, (b) Transmitted & received signals for dermis without methanol, (c) Transmitted & received signals for dermis with methanol, (d) Transmitted & received signals for epidermis with glutaraldehyde

Like SOS, the attenuation coefficient should increase linearly with the increasing concentration of gelatin powder and BSA. It increases by 0.01 and 0.018dB/cm/MHz for each extra percent of gelatin and BSA, respectively [15]. It also increases linearly for each layer of phantom skin with the transducer's increasing frequency. Attenuation coefficient for 30% BSA can be estimated to be 0.58dB/cm/MHz [25]. For soft tissue the value for attenuation is approximately 0.5 to 3.3dB/cm/MHz [17]. The calculated values for the attenuation coefficient of different phantom layers are much lower than the expected value given in table 12. The reasons behind this deviation in results can be using less concentration of BSA compared to other recipes, not having a proper alignment of the transducers while transmitting signals, smaller received signals due to coagulated powders as it attenuates the amplitude, and not using all chemicals mentioned in the paper followed for the experiment, etc. [15].

While recording the signal measurement for the SOS and attenuation coefficient, some samples were broken immediately after having contact with water. Therefore, it wasn't possible to record the measurements for all. The epidermis sample without glutaraldehyde was damaged entirely. Glutaraldehyde is a hardener, and it helps the gel

cross-link. Although the epidermis layer with glutaraldehyde also had some cracks and was removed from the water right after recording the measurement to avoid further damage. In this experiment, 0.05% of glutaraldehyde of the stock solution was used. To make the sample more stable, 0.1% can be added [15].

At first, the dermis sample without methanol was measured successfully with some distortion and noise in the signal. The thick layer of bubble on the top of the sample is the main reason for this considerable distortion. The dermis layer with methanol was a clear gel form compared to without methanol; therefore, the signal was better than the previous signal shown in figure 25.

Both the hypodermis sample with and without methanol were not firm gel shown in figure 26; therefore, no measurement was possible. The reason can be the percentage of gelatin (2%) and agar (0.2%) was relatively low, and the percentage amount of added BSA (3.33%) was significantly less compared to the paper's method (15%) followed for this experiment [15]. However, a cross-linker such as glutaraldehyde or formaldehyde might be helpful.



Figure 26: Damaged phantom sample

Different phantom layers had some coloration differences shown in figure 9. The amount of gelatin and BSA powers is the reason for it. In some layers, these chemicals were high

in amount compared to other layers. The coloration of samples does not affect the energy transfer. However, if someone wants to achieve optical properties of human skin in the same preparation, it is a significant matter of consideration.

The primary purpose of this experiment was to prepare a multilayer phantom skin and compare the procedure with the homogeneous phantom skin method. A multilayer skin model is more reliable and comparable to human skin as human skin has several layers. Different layers of skin have some deviation in properties, too. Therefore, it is more likely to modify the concentration of chemicals to achieve the desired variation of properties in separate layers. A homogeneous skin fabrication model is less challenging and sometimes easy to experiment with a new device. In contrast, heterogeneous phantom skin will help to get accurate measurements in the research.

Most of the chemicals used in preparing phantom skins are available and cheap. Among all substances, agar and gelatin are easy to fabricate inside the lab and non-hazardous. Glutaraldehyde and formaldehyde have some hazardous properties; therefore, those chemicals were used inside the fume hood with proper precautions.

6.5 Proposed multilayer phantom skin model with acoustic and electrical properties

For this research work, multilayer phantom skin is desirable, and different chemicals can be used to achieve similar electrical and acoustic properties of human skin. A repeatable method of different layers of phantom skin has been proposed here.

The epidermis layer is not so complicated to prepare as it requires fewer chemicals compared to other layers. The preparation method for the epidermis phantom proposed by Alvin I. Chena, Max L. Balter, Melanie I. Chen, Daniel Gross, Sheikh K. Alam, Timothy J. Maguire, and Martin L. Yarmush is an easy method to follow [15]. Therefore, using 5% gelatin of the total volume with 0.1% glutaraldehyde will help fabricate the epidermis layer. While preparing the solution, the glutaraldehyde should be added at the beginning to help the cross-linking of the phantom sample [16]. Later gelatin powder can be added

slowly to mix appropriately without any clumps at 45°C, which has been proven to dissolve nicely during the homogeneous phantom preparation in the lab.

The dermis phantom layer is challenging to prepare a clump-free clear solution as it requires a vast amount of gelatin powder. Instead of using both agar and gelatin powder, only using gelatin will be easy to prepare. The method proposed by O'tega A. Ejofodomi, Vesna Zderic, and Jason M. Zara can be followed to fabricate dermis phantom [25]. In this case, 10% of gelatin solution can be prepared using the same method as epidermis in terms of mixing the powder, and afterward, 30% of BSA can be added slowly at 30°C. Instead of BSA, graphite can also be used to see the difference [27]. Glutaraldehyde or formaldehyde (0.1%) can be used as a cross-linker. The fabricated dermis layer in the lab was strong without any cross-linker; it consisted of a vast amount of gelatin, which created many clumps and bubbles. Using less amount of gelatin with cross-linker can be beneficial here.

The hypodermis sample prepared in the lab was breakable; therefore, the most important thing for this layer is to use a cross-linker along with a similar process to the dermis layer. The hypodermis is the fat tissue layer of skin; thus, the phantom hypodermis layer should be less firm than the other two layers. In this case, 0.1% glutaraldehyde will be helpful to see the strength. The method proposed by Alvin I. Chena, Max L. Balter, Melanie I. Chen, Daniel Gross, Sheikh K. Alam, Timothy J. Maguire, and Martin L. Yarmush can also be used to fabricate a hypodermis phantom layer where 5 to 8% of gelatin can be used instead of 2% gelatin as the prepared hypodermis phantoms in the lab were breakable, and to achieve acoustic properties 15% BSA can be added to it [15].

With the proposed phantom layers, 171mMol NaCl solution can be added to achieve the conductivity of human skin. If the amount of solution (13ml) used in the lab experiment makes the phantom sample fragile, adhesion of a cross-linker can be a solution to it. This proposed method for phantom layered skin preparation will help fabricate more mechanically feasible phantom skins with desired electrical and acoustic properties.

6.6 Challenges and suggestions

The challenges for layered phantom fabrication are to customize and characterize such thin layers comparable with human skin, minimize the created air bubbles in the phantom gel, and track the temperature while adding modifier chemicals in specific temperatures and handling the chemicals properly inside the lab. The adding percentage of agar/gelatin powder needs special attention, or else the sample may break during the characterization of the properties. Removing the sample from the mold or petri dish is also difficult to avoid any breakage; therefore, it needs special care to remove the sample with a metal spatula. The created air bubbles can also make it challenging to get the proper signal. Therefore, a homogeneous bubble-free sample is required to get better signals. It can be achieved by following the correct procedure for sample preparation, such as adding the gelatin/agar powder at a higher temperature instead of room temperature. Then, heating the solution around 60°C instead of boiling temperature. Moreover, a pressure chamber can be used to minimize any created air bubbles in the solution [16].

Selecting the proper ultrasound transducer was also a matter of consideration. The used transducer for most of the researches were two single-element transducers in the MHz range. There are some physiological risks at high sound pressure, such as heating of the skin, cavitation in blood vessels, etc. [55]. Therefore, while selecting a transducer in this range, one should keep the health risk in mind. Secondly, insulating the transducer with PDMS was a significant concern as it may shift the transducer's resonance frequency. Moreover, a long-term insulation process is required to avoid any connection failure while measuring the signal. PDMS insulation failed during the second measurement; therefore, different biocompatible insulating materials can be used to insulate the transducer, such as Loctite 21HP, Loctite 4305, etc. [56], [57].

The measurement setup for measuring the acoustic properties was established with the available tools in the laboratory. Customized tools, such as three-dimensional (3D) printed holders can be used to improve the quality and repeatability of the test. In the experiment setup, the transducers were held by taping with plastic holders, and there was a slight bent on the upper side of the transducers due to wiring displayed in figure 20a. It wasn't easy to align both the transducers perfectly and hold the sample between

the transducer without a curvature. Therefore, a reliable holder design for the sample and transducer has been proposed for future work, shown in figure 27 and figure 28. This model for the holders will help achieve a straight and aligned position for the sample and transducers. Thus, the model shown in figure 28 can be the desired model, and it can be easily 3D printed with proper measurements. This design will help to hold the sample and transducer without any curvature, and it will also help to have an appropriate alignment between them to transfer the maximum signal.

An ideal method for the measurement setup is illustrated in figure 28, which can help avoid any signal loss in the medium. The sample should be closely attached to the transmitter and receiver signal in the beam path for this setup. The holders for the sample and transducer can be moved closer to achieve an ideal model by avoiding any gap.

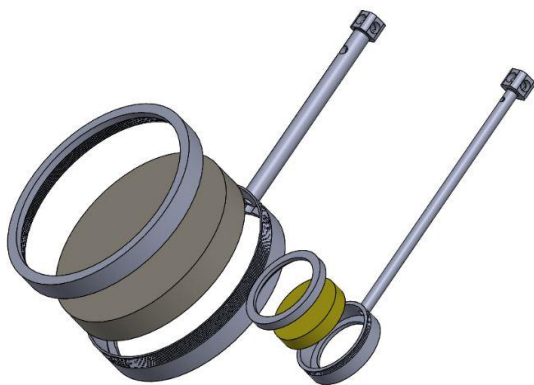


Figure 27a: Holder design for sample and transducer



Figure 27b: Holders with transducer and sample attached in it

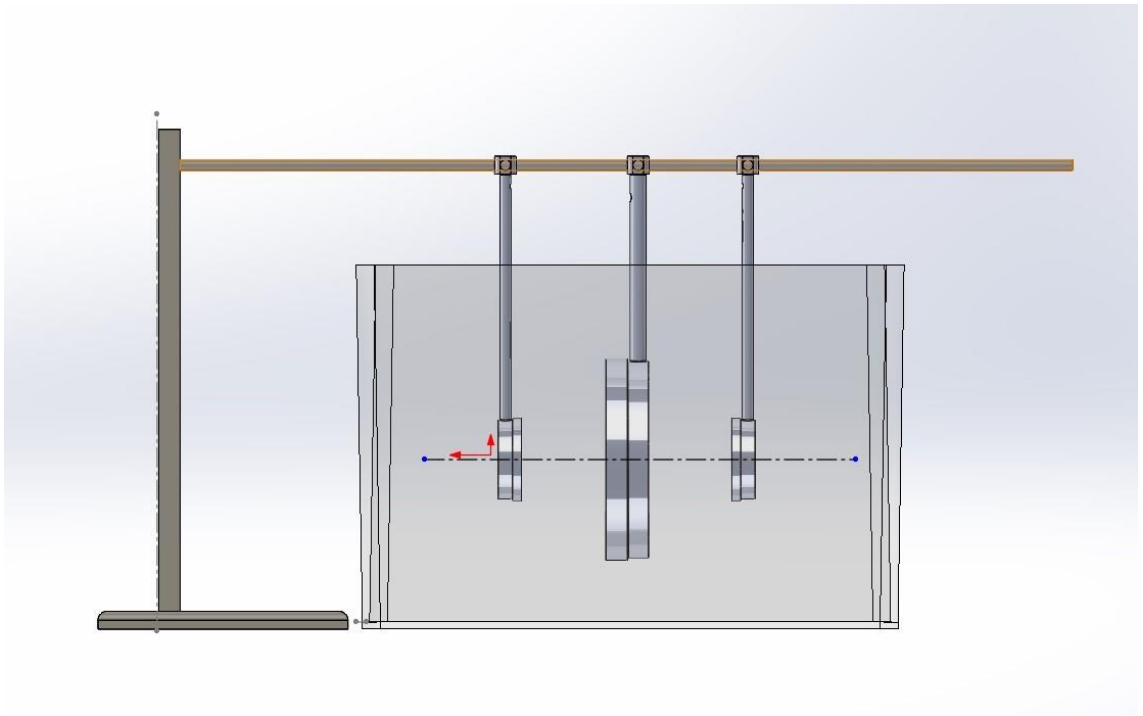


Figure 28a: Side view of the measurement setup

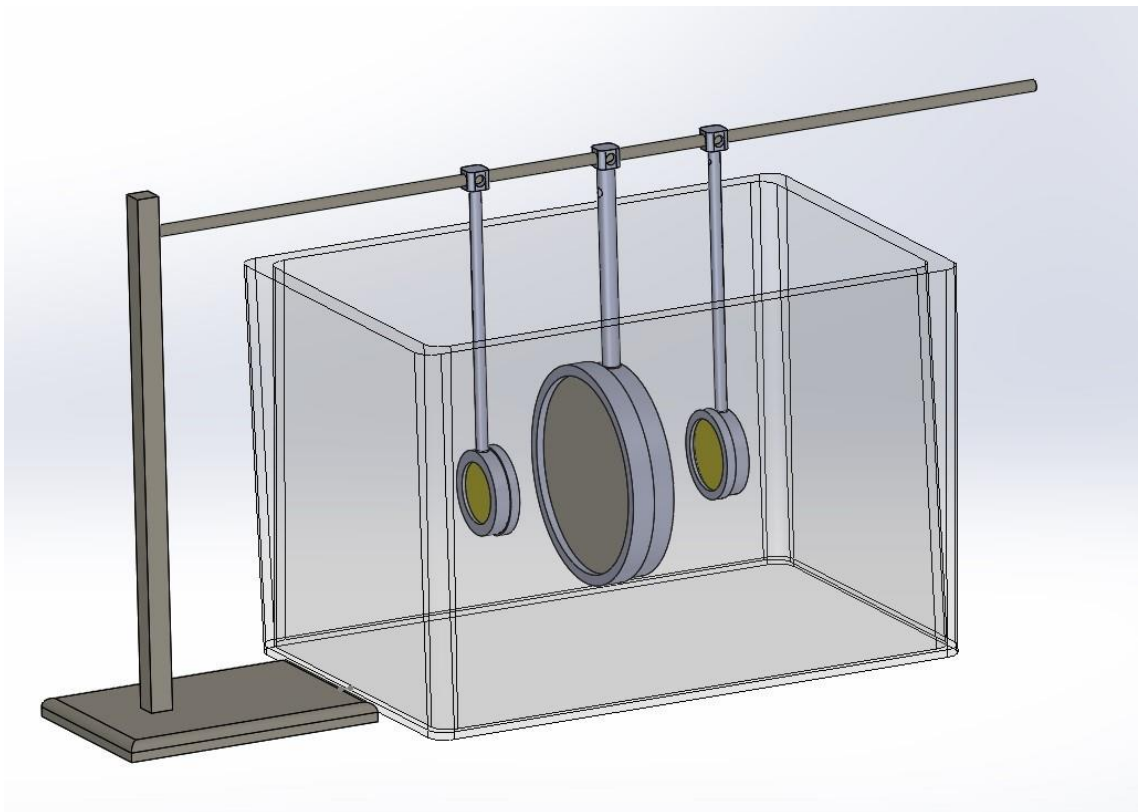


Figure 28b: 3D view of the measurement setup

7 Conclusion

The research of tissue-mimicking phantom skin is essential for biomedical technology. Before applying any novel biomedical device, it needs to be tested for safety purposes. Phantom skin with similar human skin properties is one of the best ways to test the device.

Different methods and chemicals have been suggested by researchers to fabricate phantom skin. The chemicals chosen in this experiment to replicate the human skin were suitable from various aspects, such as cheap, non-hazardous, available, etc. The result to prepare a phantom skin with similar electrical properties came out nicely. The main challenge was to prepare the multilayer phantom skin with similar acoustic properties to human skin. The obtained results for the SOS and attenuation coefficients have some deviation compared to the values of real human skin [15]. However, the concentrations of chemicals can be varied while preparing phantom skin to realize the changes in properties to get the correct concentration level for each layer of the phantom. As the amount of BSA mentioned in the paper followed for this experiment was high to dissolve properly in the solution without any clotting, an attempt can be made to use other chemicals, such as graphite, silicon carbide, Al_2O_3 , which also help to increase the attenuation coefficient. Graphite can raise the attenuation coefficient from 0.2 to 1.5 dB/cm/MHz [27]. Therefore, desired attenuation coefficients can be obtained with varying concentrations of graphite powder [54].

Bubbles and coagulated chemicals inside the gel are considerable obstacles to transfer energy or signal through the sample as the prepared gel should be homogeneous. Using a slow mixture procedure at the correct temperature can be a solution to avoid the bubbles. Moreover, a pressure chamber can also be used to minimize the bubbles. To preserve the phantom skin for a long time, antibacterial chemicals can be used, such as german plus, p-methyl, p-propyl benzoin, benzalkonium chloride, etc. [15], [19], [28].

For long-lasting stability in the insulation of the piezoelectric transducers, any biocompatible glue or epoxy can be used to have stronger adhesion of the insulating

material. On the other hand, a different waterproof transducer in MHz frequency can also be chosen.

References

- [1] A. Ben Amar, A. B. Kouki, and H. Cao, "Power Approaches for Implantable Medical Devices," *Sensors (Basel)*, vol. 15, no. 11, pp. 28889–28914, Nov. 2015, doi: 10.3390/s151128889.
- [2] B. DeLong, C. C. Chen, and J. L. Volakis, "Wireless energy harvesting for medical applications," in *2015 IEEE International Symposium on Antennas and Propagation USNC/URSI National Radio Science Meeting*, Jul. 2015, pp. 1213–1213. doi: 10.1109/APS.2015.7304995.
- [3] N. Khan and F. Khan, *RF Energy Harvesting for Portable Biomedical Devices*. 2019. doi: 10.1109/INMIC48123.2019.9022759.
- [4] H. Le, N. Fong, and H. C. Luong, "RF energy harvesting circuit with on-chip antenna for biomedical applications," in *International Conference on Communications and Electronics 2010*, Aug. 2010, pp. 115–117. doi: 10.1109/ICCE.2010.5670693.
- [5] M. Haerinia, "A State of Art Review on Wireless Power Transmission Approaches for Implantable Medical Devices," *arXiv:2003.01240 [eess]*, Mar. 2020, Accessed: May 15, 2021. [Online]. Available: <http://arxiv.org/abs/2003.01240>
- [6] R. V. Taalla, Md. S. Arefin, A. Kaynak, and A. Z. Kouzani, "A Review on Miniaturized Ultrasonic Wireless Power Transfer to Implantable Medical Devices," *IEEE Access*, vol. 7, pp. 2092–2106, 2019, doi: 10.1109/ACCESS.2018.2886780.
- [7] M. A. Hannan, S. Mutashar, S. A. Samad, and A. Hussain, "Energy harvesting for the implantable biomedical devices: issues and challenges," *BioMedical Engineering OnLine*, vol. 13, no. 1, p. 79, Jun. 2014, doi: 10.1186/1475-925X-13-79.
- [8] "Post Marketing Clinical Follow-Up (PMCF)," *Purdie Pascoe*. <https://www.purdiepascoe.com/post-marketing-clinical-followup-pmcf> (accessed May 20, 2021).
- [9] N. R. C. (US) C. on Dogs, *Criteria for Selecting Experimental Animals*. National Academies Press (US), 1994. Accessed: May 12, 2021. [Online]. Available: <https://www.ncbi.nlm.nih.gov/books/NBK236591/>
- [10] Read "Rodents" at NAP.edu. doi: 10.17226/2119.
- [11] A. AKHTAR, "The Flaws and Human Harms of Animal Experimentation," *Camb Q Healthc Ethics*, vol. 24, no. 4, pp. 407–419, Oct. 2015, doi: 10.1017/S0963180115000079.
- [12] "Shop By Phantom Type Soft Tissue Masses." https://www.bluephantom.com/category/By-Phantom-Type_Soft-Tissue-Masses.aspx (accessed May 24, 2021).
- [13] "Multi-Purpose Tissue / Cyst Ultrasound Phantom | Fluke Biomedical." <https://www.flukebiomedical.com/products/radiation-measurement/phantoms-test-tools/multi-purpose-tissue-cyst-ultrasound-phantom> (accessed May 24, 2021).
- [14] K. Zell, J. I. Sperl, M. W. Vogel, R. Niessner, and C. Haisch, "Acoustical properties of selected tissue phantom materials for ultrasound imaging," *Phys Med Biol*, vol. 52, no. 20, pp. N475–484, Oct. 2007, doi: 10.1088/0031-9155/52/20/N02.
- [15] A. I. Chen *et al.*, "Multilayered tissue mimicking skin and vessel phantoms with tunable mechanical, optical, and acoustic properties," *Med Phys*, vol. 43, no. 6, pp. 3117–3131, Jun. 2016, doi: 10.1118/1.4951729.
- [16] J. R. Cook, R. R. Bouchard, and S. Y. Emelianov, "Tissue-mimicking phantoms for photoacoustic and ultrasonic imaging," *Biomed Opt Express*, vol. 2, no. 11, pp. 3193–3206, Oct. 2011, doi: 10.1364/BOE.2.003193.

- [17] M. E. Rabie, M. F. Ahmed, A. D. Mann, and S. J. Singhal, "Ultrasound Tissue Mimicking Materials Using 2% Agar based phantom," *The International Conference on Electrical Engineering*, vol. 9, no. 9th International Conference on Electrical Engineering ICEENG 2014, pp. 1–7, May 2014, doi: 10.21608/iceeng.2014.30467.
- [18] G. Deng, L. Cai, J. Feng, S. Duan, P. Zhang, and S. X. Xin, "Reliable Method for Fabricating Tissue-Mimicking Materials With Designated Relative Permittivity and Conductivity at 128MHz," *Bioelectromagnetics*, vol. 42, no. 1, pp. 86–94, Jan. 2021, doi: 10.1002/bem.22303.
- [19] M. O. Culjat, D. Goldenberg, P. Tewari, and R. S. Singh, "A review of tissue substitutes for ultrasound imaging," *Ultrasound Med Biol*, vol. 36, no. 6, pp. 861–873, Jun. 2010, doi: 10.1016/j.ultrasmedbio.2010.02.012.
- [20] L. Elvira *et al.*, "Development and Characterization of Medical Phantoms for Ultrasound Imaging Based on Customizable and Mouldable Polyvinyl Alcohol Cryogel-Based Materials and 3-D Printing: Application to High-Frequency Cranial Ultrasonography in Infants," *Ultrasound Med Biol*, vol. 45, no. 8, pp. 2226–2241, Aug. 2019, doi: 10.1016/j.ultrasmedbio.2019.04.030.
- [21] F. Ratto *et al.*, "Hybrid organosilicon/polyol phantom for photoacoustic imaging," *Biomed Opt Express*, vol. 10, no. 8, pp. 3719–3730, Aug. 2019, doi: 10.1364/BOE.10.003719.
- [22] D. Bennett, "NaCl doping and the conductivity of agar phantoms," 2011, doi: 10.1016/J.MSEC.2010.08.018.
- [23] T. J. Hall, M. Bilgen, M. F. Insana, and T. A. Krouskop, "Phantom materials for elastography," *IEEE Transactions on Ultrasonics, Ferroelectrics and Frequency Control*, vol. 44, no. 6, pp. 1355–1365, Dec. 1997, doi: 10.1109/58.656639.
- [24] E. L. Madsen *et al.*, "Interlaboratory comparison of ultrasonic backscatter, attenuation, and speed measurements," *J Ultrasound Med*, vol. 18, no. 9, pp. 615–631, Sep. 1999, doi: 10.7863/jum.1999.18.9.615.
- [25] "3. Tissue-mimicking bladder wall phantoms for evaluating acoustic radiation force—optical coherence elastography systems O'tega A. Ejofodomi, a Vesna Zderic, and Jason M. Zara Department of Electrical and Computer Engineering, George Washington University, Washington D.C. 20052".
- [26] J. H. Park, J. A. Jackman, A. R. Ferhan, G. J. Ma, B. K. Yoon, and N.-J. Cho, "Temperature-Induced Denaturation of BSA Protein Molecules for Improved Surface Passivation Coatings," *ACS Appl Mater Interfaces*, vol. 10, no. 38, pp. 32047–32057, Sep. 2018, doi: 10.1021/acsami.8b13749.
- [27] E. L. Madsen, J. A. Zagzebski, R. A. Banjavie, and R. E. Jutila, "Tissue mimicking materials for ultrasound phantoms," *Med Phys*, vol. 5, no. 5, pp. 391–394, Oct. 1978, doi: 10.1118/1.594483.
- [28] "Tissue-mimicking materials for elastography phantoms: A review - ScienceDirect." <https://www.sciencedirect.com/science/article/pii/S2352431617301487> (accessed Apr. 21, 2021).
- [29] K. Zell, J. I. Sperl, M. W. Vogel, R. Niessner, and C. Haisch, "Acoustical properties of selected tissue phantom materials for ultrasound imaging," *Phys Med Biol*, vol. 52, no. 20, pp. N475-484, Oct. 2007, doi: 10.1088/0031-9155/52/20/N02.
- [30] M. Hoffman and MD, "The Skin (Human Anatomy): Picture, Definition, Function, and Skin Conditions," *WebMD*. <https://www.webmd.com/skin-problems-and-treatments/picture-of-the-skin> (accessed Apr. 20, 2021).

- [31] J. Sandby-Møller, T. Poulsen, and H. C. Wulf, "Epidermal thickness at different body sites: relationship to age, gender, pigmentation, blood content, skin type and smoking habits," *Acta Derm Venereol*, vol. 83, no. 6, pp. 410–413, 2003, doi: 10.1080/00015550310015419.
- [32] "A simple and accurate FDTD based technique to determine equivalent complex permittivity of the multi-layered human tissue in MICS band | Elsevier Enhanced Reader." <https://reader.elsevier.com/reader/sd/pii/S2468217920300137?token=DA8A61988069F16D824A4547C56F93C04C305AED7BFBF11667174D53EE77308FCBD6D129834ED48BE656919BF7AE893E&originRegion=eu-west-1&originCreation=20210424083240> (accessed Apr. 24, 2021).
- [33] K. Wake, K. Sasaki, and S. Watanabe, "Conductivities of epidermis, dermis, and subcutaneous tissue at intermediate frequencies," *Phys. Med. Biol.*, vol. 61, no. 12, pp. 4376–4389, May 2016, doi: 10.1088/0031-9155/61/12/4376.
- [34] N. M. Tamyis, D. K. Ghodgaonkar, M. N. Taib, and W. T. Wui, "DIELECTRIC PROPERTIES OF HUMAN SKIN IN VIVO IN THE FREQUENCY RANGE 18-40 GHz," p. 4.
- [35] Y. Yu, A. Lowe, G. Anand, and A. Kalra, "Tissue phantom to mimic the dielectric properties of human muscle within 20 Hz and 100 kHz for biopotential sensing applications," in *2019 41st Annual International Conference of the IEEE Engineering in Medicine and Biology Society (EMBC)*, Jul. 2019, pp. 6490–6493. doi: 10.1109/EMBC.2019.8856530.
- [36] "How the Radio Spectrum Works," *HowStuffWorks*, Apr. 01, 2000. <https://electronics.howstuffworks.com/radio-spectrum.htm> (accessed May 23, 2021).
- [37] "How does radio frequency work?," *Telectronic*, Oct. 01, 2015. <https://telectronica.com/como-funciona-la-radiofrecuencia/> (accessed May 23, 2021).
- [38] "Electrolytes, ionisation and conductivity | Reactions in aqueous solution | Siyavula." <https://intl.siyavula.com/read/science/grade-10/reactions-in-aqueous-solution/18-reactions-in-aqueous-solution-03> (accessed May 16, 2021).
- [39] A. Abd Ali, H. Fadhil, E. Yousif, Z. Hussain, S. Abdul-Wahab, and D. Zageer, "An Insight Into Measuring Conductivity Of Solutions With Ease: A Review," *Research Journal of Pharmaceutical, Biological and Chemical Sciences*, vol. 8, pp. 2033–2037, Mar. 2017.
- [40] "Definition of resonant circuit | Dictionary.com," [www.dictionary.com](https://www.dictionary.com/browse/resonant-circuit), <https://www.dictionary.com/browse/resonant-circuit> (accessed May 30, 2021).
- [41] M. Fredrik Walaas, "Skin Conductivity Hydration Monitoring for Wearable Devices."
- [42] B. Zeqiri, W. Scholl, and S. P. Robinson, "Measurement and testing of the acoustic properties of materials: a review," *Metrologia*, vol. 47, no. 2, pp. S156–S171, Mar. 2010, doi: 10.1088/0026-1394/47/2/S13.
- [43] A. Souza, J. Ribeiro, and F. Araújo, "Study of PDMS characterization and its applications in biomedicine: A review," *Journal of Mechanical Engineering and Biomechanics*, vol. 4, pp. 1–9, Aug. 2019, doi: 10.24243/JMEB/4.1.163.
- [44] "Polydimethylsiloxane material as hydrophobic and insulating layer in electrowetting-on-dielectric systems," *Microelectron. J.*, vol. 45, no. 12, pp. 1684–1690, Dec. 2014, doi: 10.1016/j.mejo.2014.05.016.
- [45] J. Friend and L. Yeo, "Fabrication of microfluidic devices using polydimethylsiloxane," *Biomicrofluidics*, vol. 4, no. 2, Mar. 2010, doi: 10.1063/1.3259624.

- [46] "Minimum & Maximum Impedance." <https://www.americanpiezo.com/knowledge-center/piezo-theory/determining-resonance-frequency.html> (accessed Apr. 20, 2021).
- [47] K. Ono, "A Comprehensive Report on Ultrasonic Attenuation of Engineering Materials, Including Metals, Ceramics, Polymers, Fiber-Reinforced Composites, Wood, and Rocks," *Applied Sciences*, vol. 10, p. 2230, Mar. 2020, doi: 10.3390/app10072230.
- [48] S. Zhang, H. Jeong, S. Cho, and X. Li, "Measurement of attenuation coefficients of the fundamental and second harmonic waves in water," *AIP Conference Proceedings*, vol. 1706, no. 1, p. 060011, Feb. 2016, doi: 10.1063/1.4940517.
- [49] W. Zhang, X. Chen, Y. Wang, L. Wu, and Y. Hu, "Experimental and Modeling of Conductivity for Electrolyte Solution Systems," *ACS Omega*, vol. 5, no. 35, pp. 22465–22474, Sep. 2020, doi: 10.1021/acsomega.0c03013.
- [50] "Norway," *Sigma-Aldrich*. <https://www.sigmaaldrich.com/norway.html> (accessed May 10, 2021).
- [51] G.-L. Luo, Y. Kusano, and D. Horsley, *Immersion PMUTs Fabricated with a Low Thermal-Budget Surface Micromachining Process*. 2018. doi: 10.1109/ULTSYM.2018.8579826.
- [52] D. Amrani, "A comparative study of sound speed in air at room temperature between a pressure sensor and a sound sensor," *Phys. Educ.*, vol. 48, no. 1, pp. 65–71, Dec. 2012, doi: 10.1088/0031-9120/48/1/65.
- [53] M. Chávez, V. Sosa, and R. Tsumura, "Speed of sound in saturated pure water," *Journal of The Acoustical Society of America - J ACOUST SOC AMER*, vol. 77, pp. 420–423, Feb. 1985, doi: 10.1121/1.391861.
- [54] D. Oliveira *et al.*, *ACOUSTIC AND THERMAL PROPERTIES IN AGAROSE-BASED PHANTOM WITH DIFFERENT GRAPHITE POWDER CONCENTRATION*. 2014.
- [55] "Exponent - Ultrasound in Consumer Products." <https://www.exponent.com/knowledge/thought-leadership/2019/ultrasound-in-consumer-products> (accessed May 28, 2021).
- [56] "LOCTITE EA M-21HP." https://www.henkel-adhesives.com/us/en/product/structural-adhesives/loctite_ea_m-21hp.html (accessed May 28, 2021).
- [57] "LOCTITE 4305." https://www.henkel-adhesives.com/ch/en/product/uv-curing-adhesives/loctite_4305.html (accessed May 28, 2021).
- [58] https://people.rit.edu/lffeee/CD4007_SPICE_MODEL.pdf

List of figures

Figure 1: Human skin layers with thickness.....	15
Figure 2: Electrical model of the ultrasound transducer and RF antenna.....	18
Figure 3: Vibration mode of piezoelectric disc transducer.....	19
Figure 4: Circuit diagram of transmitting transducer connected to the driver.....	20
Figure 5: NaCl solution with different concentrations, and the calculation is given in table 2.....	23
Figure 6: Agar gel with NaCl.....	24
Figure 7: Multimeter used for resistance measurement.....	25
Figure 8: (a) Conductivity meter, (b) Measuring the conductivity of the solution with the probe.....	25
Figure 9: Different phantom gel layers in petry dishes.....	28
Figure 10: Phantom skin sample on the hotplate (turned on) covered with a lid to avoid evaporation of the chemical solution.....	30
Figure 11: Characterization of phantom skin model.....	30
Figure 12: Front and rear sides of the piezoelectric transducer.....	31
Figure 13: Piezoelectric transducer with silicone cover.....	32
Figure 14: Impedance Vs. frequency graph (f_s is the resonance frequency & f_p is the anti-resonance frequency) [46].....	33
Figure 15: Network analyzer for impedance measurement.....	33
Figure 16: Circuit diagram of CD 4007UBE [58].....	34
Figure 17: Circuit design for the driver.....	34
Figure 18: PCB layout of the driver.....	35
Figure 19: Schematic of the experimental setup for the acoustic measurement.....	35
Figure 20: (a) Phantom sample in the beam path; (b) Extraction of the sample with a metal spatula.....	36
Figure 21: Change in the conductivity with varying concentrations of NaCl.....	41
Figure 22: The conductivity comparison with varying amounts of NaCl solution.....	41
Figure 23: (a) Transmitter's resonance frequency before PDMS, (b) Transmitter's resonance frequency after PDMS, (c) Receiver's resonance frequency before PDMS, (d) Receiver's resonance frequency after PDMS.....	44

Figure 24: (a) Transmitted & received signals in the water, (b) Transmitted & received signals for epidermis with glutaraldehyde, (c) Transmitted & received signals for dermis without methanol, (d) Transmitted & received signals for dermis with methanol.....	46
Figure 25: (a) Transmitted & received signals in the water, (b) Transmitted & received signals for dermis without methanol, (c) Transmitted & received signals for dermis with methanol, (d) Transmitted & received signals for epidermis with glutaraldehyde.....	51
Figure 26: Damaged phantom sample.....	52
Figure 27a: Holder design for sample and transducer.....	56
Figure 27b: Holders with transducer and sample attached in it.....	56
Figure 28a: Side view of the measurement setup.....	57
Figure 28b: 3D view of the measurement setup.....	57

List of tables

Table 1: Comparison between ultrasound and RF energy transfer methods.....	9
Table 2: Thickness of different skin layers [15], [31].....	16
Table 3: Chemical composition of phantom skin to obtain target conductivity.....	22
Table 4: Agar gel preparation with NaCl solution.....	24
Table 5: Chemical composition of phantom skin layers to obtain the target acoustic properties in the lab.....	28
Table 6: Amount of different chemical for agar gel preparation.....	29
Table 7: Measured conductivity with the multimeter (DMM6500) of different solutions.....	39
Table 8: Measured conductivity with the conductivity meter (1410-1002) of different NaCl with agar gel solutions.....	39
Table 9: Resonance frequency of the transducers.....	42
Table 10: Speed of sound of the phantom samples.....	47
Table 11: Time delay calculations from different papers.....	48
Table 12: Attenuation coefficient of different samples.....	49

Appendix

Appendix 1: MATLAB script for amplitude

```
clc;
clear all;
close all;

%font setup instruction
set(0,'DefaultTextFontName','Times',...
'DefaultTextFontSize',20,...
'DefaultAxesFontName','Times',...
'DefaultAxesFontSize',20,...
'DefaultLineLineWidth',1,...
'DefaultLineMarkerSize',7.75)

M = csvread('test file.csv',2,0); %EXTRACT DATA FROM CSV FILE

%measurement only water 9cm distance between TX and RX
time=M(:,1);
vin=M(:,2);
vout=M(:,3);

figure(1)

subplot(311)
plot(time,vin)
xlabel('time (s)')
ylabel('VTX (V)')
grid on
title('sample title : test\_water.csv')
xlim([-0.1e-4,1e-4])
subplot(312)
plot(time,vout)
xlabel('time (s)')
ylabel('VRX (V)')
grid on
xlim([-0.1e-4,1e-4])
subplot(313)
yyaxis left
plot(time,vout,'k')
ylabel('VRX (V)')
yyaxis right
xlim([-0.1e-4,1e-4])
plot(time,vin,'r')
xlabel('time (s)')
ylabel('VTX (V)')
grid on
```

```
xlim([-0.1e-4,1e-4])
```

Appendix 2: MATLAB code for time delay (processed data)

```
M = csvread('test file.csv',2,0); %EXTRACT DATA FROM CSV FILE
```

```
time=M(:,1);  
vin=M(:,2);  
vout=M(:,3);
```

```
figure(6)  
subplot(311)  
plot(time,vin)  
xlabel('time (s)')  
ylabel('VTX (V)')  
grid on  
title('Sample title: zoom\_test\_water.csv')  
xlim([-0.05e-4,0.9e-4])  
subplot(312)  
xlim([-0.05e-4,0.9e-4])  
subplot(312)  
plot(time,vout)  
xlabel('time (s)')  
ylabel('VRX (V)')  
grid on  
xlim([-0.05e-4,0.9e-4])  
subplot(313)  
yyaxis left  
plot(time,vout,'k')  
ylabel('VRX (V)')  
yyaxis right  
xlim([-0.05e-4,0.9e-4])  
plot(time,vin,'r')  
xlabel('time (s)')  
ylabel('VTX (V)')  
grid on  
xlim([-0.05e-4,0.9e-4])
```

```
x=1e-15;  
y2 = lowpass(lowpass(lowpass(lowpass(vout,x),x),x),x);  
y2 = highpass(y2,0.003);  
y2(find(time<60e-6))=0;  
y2(find(y2>0.0028))=1; % threshold just above the background noise  
y2(find(y2<-0.0028))=-1; % just below background noise  
y2(find(time<60e-6))=0;  
figure(10)  
plot(time,y2,'k')
```

```
hold on
plot(time,vin-4.99,'r')
```

Appendix 3: MATLAB code for resonance frequency

```
function PlotImpedance_Mod(trace)
```

```
%SCRIPT FOR PLOTTING ELECTRICAL IMPEDANCE FILES FROM NETWORK ANALYSER
```

```
Zref = 50;           % Ohm Reference impedance
```

```
%--- Load raw data ---
```

```
%tracefile='3-1comp_before_1.trc'
```

```
tracefile='file.trc' % .trc FILE FROM PATH
```

```
%tracefile='413_L2_air.trc' % .trc FILE FROM PATH
```

```
trc= readtrace(tracefile);
```

```
%--- Create frequency vector, calculate Z, and plot impedance ---
```

```
f= [0:trc.Np-1]*trc.dx+trc.x0; % Hz Frequency vector
```

```
S11 = double(trc.y(:,1)+ 1i*trc.y(:,2));
```

```
Z = Zref* (1+S11)./(1-S11); % Ohm Complex impedance
```

```
figure(55)
```

```
%Titlename='L.trc';
```

```
color='m';
```

```
Cap=-1./((2*pi).*f.*imag(Z));
```

```
subplot(2,2,1)
```

```
hold on;
```

```
semilogy(f./1e6,abs(Z),color);
```

```
xlabel('Frequency [MHz]')
```

```
ylabel('Impedance magnitude [Ohm]')
```

```
%title(Titlename)
```

```
grid on
```

```
subplot(2,2,3)
```

```
hold on;
```

```
phi = angle(Z);
```

```
plot(f./1e6,rad2deg(phi),color);
```

```
xlabel('Frequency [MHz]')
```

```
ylabel('Phase [deg]')
```

```
ylim([-90 90])
```

```
%xlim([0 20])
```

```
set(gca, 'ytick', [-90:20:90])
```

```

grid on

% subplot(2,2,2)
% hold on;
% semilogy(f./1e6,real(Z),color);
% xlabel('Frequency [MHz]')
% ylabel('Real Z Value [Ohm]')
% ylim([0 600])
% xlim([0 20])
% grid on

subplot(2,2,2)
hold on;
plot(f./1e6,Cap./1e-9,color);
xlabel('Frequency [MHz]')
ylabel('Capacitance [nF]')

grid on

subplot(2,2,4)
hold on;
plot(f./1e6,imag(Z),color);
xlabel('Frequency [MHz]')
ylabel('Imaginary [Ohm]')
ylim([-300 300])
grid on

set(gcf,'color','w')

%---Use to set legend
% h= legend('Housing','Wire')
% v=get(h,'Title')
% set(v,'string','8MHz Transducer')

return

```

Appendix 4: Complete setup for acoustic measurement in the lab

